1995-09

High frequency subsurface Lagrangian measurements in the California Current with RAFOS floats

Benson, Kirk R.

Monterey, California. Naval Postgraduate School

NAVAL POSTGRADUATE SCHOOL
MONTEREY, CALIFORNIA

THESIS

HIGH FREQUENCY SUBSURFACE LAGRANGIAN MEASUREMENTS IN THE CALIFORNIA CURRENT WITH RAFOS FLOATS

by

Kirk R. Benson

September, 1995

Thesis Advisor: Newell Garfield
Second Reader: Robert G. Paquette

Approved for public release; distribution is unlimited.

DISCLAIMER NOTICE

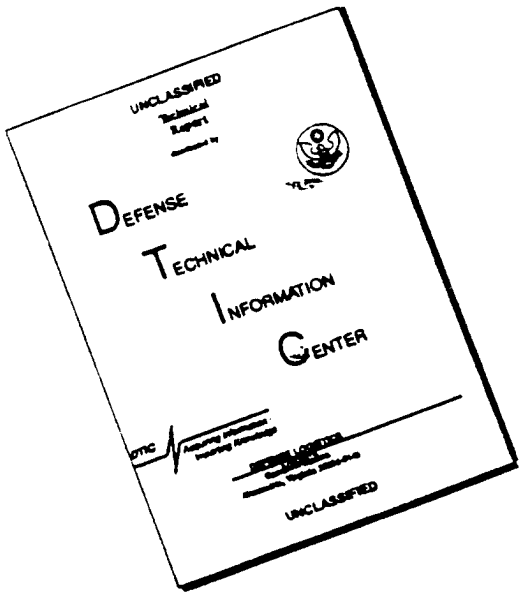

THIS DOCUMENT IS BEST QUALITY AVAILABLE. THE COPY FURNISHED TO DTIC CONTAINED A SIGNIFICANT NUMBER OF PAGES WHICH DO NOT REPRODUCE LEGIBLY.

REPORT DOCUMENTATION PAGE	Form Approved OMB No. 0704-

Public reporting burden for this collection of information is estimated to average 1 hour per response, including the time for reviewing instruction, searching existing data sources, gathering and maintaining the data needed, and completing and reviewing the collection of information. Send comments regarding this burden estimate or any other aspect of this collection of information, including suggestions for reducing this burden, to Washington Headquarters Services, Directorate for Information Operations and Reports, 1215 Jefferson Davis Highway, Suite 1204, Arlington, VA 22202-4302, and to the Office of Management and Budget, Paperwork Reduction Project (0704-0188) Washington DC 20503.

1. AGENCY USE ONLY *(Leave blank)*	2. REPORT DATE September 1995	3.REPORT TYPE AND DATES COVERED Master's Thesis

4. TITLE AND SUBTITLE High Frequency Subsurface Lagrangian Measurements in the California Current with RAFOS Floats	5. FUNDING NUMBERS
6. AUTHOR(S) Kirk R. Benson	
7. PERFORMING ORGANIZATION NAME(S) AND ADDRESS(ES) Naval Postgraduate School Monterey CA 93943-5000	8. PERFORMING ORGANIZATION REPORT NUMBER
9. SPONSORING/MONITORING AGENCY NAME(S) AND ADDRESS(ES)	10. SPONSORING/ MONITORING AGENCY REPORT NUMBER

11. SUPPLEMENTARY NOTES The views expressed in this thesis are those of the author and do not reflect the official policy or position of the Department of Defense or the U.S. Government.

12a. DISTRIBUTION/AVAILABILITY STATEMENT Approved for public release; distribution is unlimited.	12b. DISTRIBUTION CODE

13. ABSTRACT *(maximum 200 words)*

This study presents float observations from four RAFOS floats that were deployed off central California for a twenty-three day period as part of a Tomography Demonstration Experiment. These floats, which sampled hourly, were used to investigate float characteristics and the navigational accuracy of current processing techniques. An ordinary mean least square method is proposed to mathematically estimate values for random and systematic errors, producing navigational trajectories which compliment previous methods when determining the most probable solution of the float trajectory. Potential sources of error in the navigational solution are examined, as well as the importance of float/source geometry on position accuracy. It was determined that these floats supported previous studies of the California Current System, and proposes that the California Undercurrent may in fact be wider and deeper that previously suspected.

14. SUBJECT TERMS California Current, California Undercurrent, RAFOS, Lagrangian, Tomography, SOFAR, Dilution of Precision, DOP, ARGOS, Error Correction, OMLS, Ordinary Mean Least Squares	15.NUMBER OF PAGES 103
	16. PRICE CODE

17. SECURITY OF REPORT Unclassified	18. SECURITY CLASSIFICATION OF THIS PAGE Unclassified	19. SECURITY CLASSIFICATION OF ABSTRACT Unclassified	20.LIMITATION OF ABSTRACT UL
CLASSIFICATION			

NSN 7540-01-280-5500

Standard Form 298 (Rev. 2-89)
Prescribed by ANSI Std. 239-18 298-102

Approved for public release; distribution is unlimited.

HIGH FREQUENCY SUBSURFACE LAGRANGIAN MEASUREMENTS IN THE CALIFORNIA CURRENT WITH RAFOS FLOATS

Kirk R. Benson
Lieutenant, United States Navy
B.S., United States Naval Academy, 1987

Submitted in partial fulfillment
of the requirements for the degree of

MASTER OF SCIENCE IN METEOROLOGY AND PHYSICAL OCEANOGRAPHY

from the

NAVAL POSTGRADUATE SCHOOL
September 1995

Author: [redacted]
Kirk R. Benson

Approved by: [redacted]
Newell Garfield, Thesis Advisor

[redacted]
Robert G. Paquette, Second Reader

[redacted]
Robert H. Bourke, Chairman
Department of Oceanography

ABSTRACT

This study presents float observations from four RAFOS floats that were deployed off central California for a twenty-three day period as part of a Tomography Demonstration Experiment. These floats, which sampled hourly, were used to investigate float characteristics and the navigational accuracy of current processing techniques. An ordinary mean least square method is proposed to mathematically estimate values for random and systematic errors, producing navigational trajectories which compliment previous methods when determining the most probable solution of the float trajectory. Potential sources of error in the navigational solution are examined, as well as the importance of float/source geometry on position accuracy. It was determined that these floats supported previous studies of the California Current System, and proposes that the California Undercurrent may in fact be wider and deeper that previously suspected.

TABLE OF CONTENTS

LIST OF FIGURES

LIST OF TABLES

ACKNOWLEDGEMENTS

I would like to thank Dr. Toby Garfield and Dr. Robert Paquette for their support and for always having time for my numerous questions. I want to convey my appreciation to the following people as well: Mr. Tarry Rago, Mr. Mike Cook, Dr. James Clynch, Dr. Skip Carter, Mr. Chris Miller, Mr. Brian Miller and Mr. Tom Shmottlach.

Most importantly, I want to thank my wife Inger, son Phillip, and daughter Haley for their tremendous support and understanding, without which, this thesis would not have been possible.

I. INTRODUCTION

The California Current System (CCS) is the eastern limb of the North Pacific Subtropical Gyre and possesses a number of characteristics common with other eastern boundary currents. These characteristics are a broad surface equatorward flow with a deep subsurface poleward undercurrent located over the continental slope (Chelton, 1984). The CCS has been extensively studied by numerous investigators who have identified a number of features of this current system.

The most consistent and prevalent feature of the CCS is the California Current (CC). The CC is a broad, weak equatorward meandering flow that is normally shallower than 300 m. Speeds are usually less that 25 cm s^{-1}, but geostrophic observations of speeds up to 50 cm s^{-1} have been reported. The water, which is of West Wind Drift origin, has been modified by its long trip across the Pacific in its contact with Pacific Subarctic water along the Polar Front (Reece, 1989).

Eastern boundary current regions, such as the CC, are now recognized to be eddy-rich, full of strongly time-dependent and spatially structured variability in the flow field. This variability apparently received little attention until Bernstein et al. (1977) demonstrated that the complex structures so visible in satellite infrared (IR) imagery could indeed be matched to comparable variability measured through traditional in situ means (Brink and Cowles, 1991). In the CC case, however, few images from the four years of satellite data examined by Rosenfeld et al. (1994) showed meanders becoming detached eddies. Also in this variability exist cold surface filaments, typically less than 100 km wide but hundreds of kilometers long which extend offshore from the coast (Brink and Cowles, 1991).

The California Undercurrent (CUC) is a narrow poleward countercurrent that is normally located just below the main pycnocline and adjacent to the continental slope. This Pacific water is formed in the eastern tropical Pacific and is defined by relatively high temperature, high salinity, high nutrients and low dissolved oxygen (Sverdrup et al., 1942). The CUC has been observed locally from Baja California, Mexico (Wooster and Jones, 1970) to Vancouver Island, Canada (Hickey, 1979)(Figure 1), however, it's continuity has not been observed. Indirect evidence for this flow is clearly visible in the large-scale temperature-salinity characteristics of coastal waters as northward-tending tongues of relatively warm, saline water (Huyer et al., 1989). The position, depth and strength of the CUC is highly variable and can be related to seasonal changes in wind stress and wind stress curl (Hickey, 1979).

The CUC has been the subject of numerous studies which include calculations of derived geostrophic velocity, from hydrographic data and direct current measurements. Tibby (1941) found indirect evidence of the CUC by studying hydrographic sections along the west coast of North America. Direct measurements of the CUC were made by Reid (1962) off Central California by tracking parachute drogues. The core of the CUC was found at 250 m with a speed of 20 cm s^{-1}. Wooster and Jones (1970) used Richardson-type current meters and found a narrow (20 km) undercurrent with an average speed of 30 cm s^{-1} over the continental slope off Punta Colnett, Baja California, Mexico (Rischmiller, 1993).

Chelton (1984) analyzed 23 years of California Cooperative Fisheries Investigation (CalCOFI) hydrographic data off Point Sur and Point Conception. Mean geostrophic velocities for this data set indicated that the CUC has a seasonal variability off Point Sur. The CUC was found to be present from June through February with a peak velocity

occurring in December (14 cm s^{-1}). If in fact the CUC is only 20 km wide, it is probable that Chelton was limited in his study of the CUC due to the 65 km spacing of the CalCOFI hydrographic data sampling grid. Ramp et al. (1994) studied five years of current data over the upper slope off Point Sur using a single array of current meters. The period April through July was characterized by strong poleward flow. During this study, the average poleward flow was approximately north-northwest at 20 cm s^{-1}. Wickham et al. (1987) analyzed two years of current array measurements and hydrographic data near Cape San Martin, California. The variability of the CUC was found to be seasonal, except that the flow was stronger

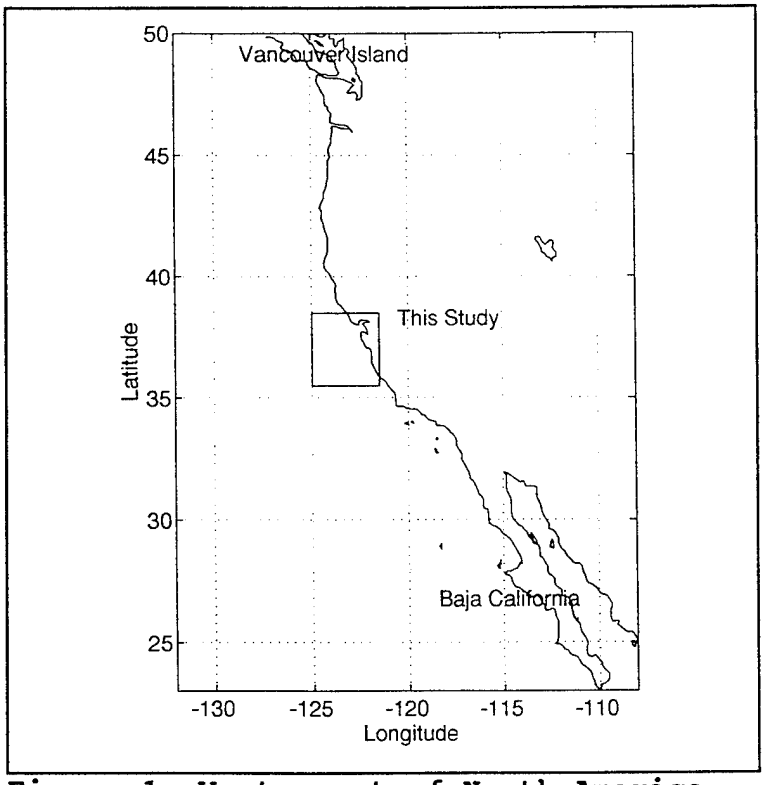

Figure 1. West coast of North America showing region of this study.

and deeper between May and June. Lynn and Simpson (1987) noted seasonal variability of the CUC off Central California in their harmonic analysis of the CalCOFI data set. Rischmiller (1993) determined that the CUC becomes weaker with a greater core depth from January to March, while from March to May it was almost nonexistent. However, Rischmiller indicated that the variability of the CUC is interannual rather that seasonal. The short duration of his data set when compared to earlier geostrophic studies and the absence of upper slope and shelf velocity data may account for the absence of a pronounced seasonal signal.

The data for this study were obtained from four RAFOS Floats (launched from the Research Vessel (RV) Point Sur) used in a Coastal Tomography Demonstration conducted by the Naval Postgraduate School (NPS) during the Spring of 1994. This demonstration actually used five floats, but the fifth float, NPS #27, failed to collect any useable data due to a failure of unknown cause in the float electronics. A RAFOS float, which will be described in detail in Chapter III, is a neutrally buoyant, primarily isobaric, subsurface drifter that measures temperature and pressure, and receives acoustic transmissions from moored sound sources for positioning determination. These RAFOS floats received and processed acoustic transmissions from three fixed submerged sound sources off Central California (Figure 2) at twenty minute intervals, respectively, producing fixes at the unusually high frequency of once per hour, instead of the usual frequency of once every eight hours. These floats also measured temperature and pressure upon the completion of each fix.

This study presents the float observations from the four floats that were operational for a twenty-three day period in May and June of 1994. These floats were deployed in the Tomography Array with the intent of using them to verify tomography measurements. Unfortunately, the tomography data

were not recovered, so no direct comparisons were made. However, the hourly fixes enable looking at higher frequency Lagrangian motion and examining the errors associated with RAFOS position determination. These two objectives are the focus of this study.

Regional characteristics will be discussed in Chapter II. Data collection and processing will be discussed in Chapter III. Analyses of the RAFOS float data are discussed in Chapter IV. The results and a comparison with earlier studies of the CCS are discussed in Chapter V. Chapter VI contains a summary of conclusions and recommendations for future work.

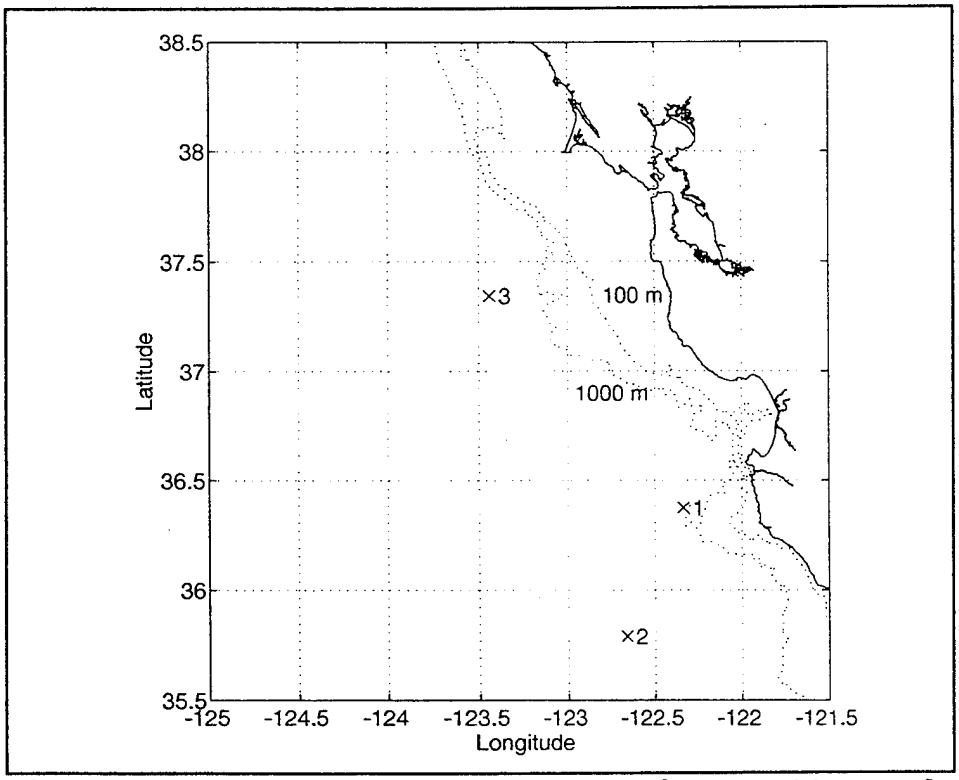

Figure 2. RAFOS sound source locations (100 m and 1000 m isobaths indicated).

II. REGIONAL CHARACTERISTICS

RAFOS floats directly measure temperature and pressure, and they measure position by acoustic ranging from moored sound sources. From position information, horizontal velocity components, u and v, can be derived, while the vertical velocity component, w, is derived from pressure measurements. These characteristics of the flow in the CUC along with salinity data are important for accurately describing the properties of the flow and allow a better understanding of the CUC.

A. TEMPERATURE AND SALINITY

Temperature is a particularly important property of seawater because with it alone, one may gain valuable insight into circulation features and sound speed distributions (Pickard and Emery, 1990). In recent studies, the average seawater temperature at 275 m (the depth of interest in this study) during May and June has been found to be 7° C (Wittman et al., 1985).

Salinity, which cannot be measured directly, is determined from measurements of electrical conductivity and temperature (Pond and Pickard, 1983). Salinity is used to determine density and sound speed. Off Central California during May and June, the average salinity at 275 m was found to be 34.00 PSU (Wittman et al., 1985).

B. SOUND SPEED

The speed of sound in the sea is given by the relation

$$C = \sqrt{1/\beta\rho} \qquad (1)$$

where β is the adiabatic compressibility of sea-water and ρ is the density. The sound speed in the ocean is a function of salinity, temperature, and pressure. According to one empirical relation by Urick (1983)

$$C = 1449 + 4.6t - 0.55t^2 + 1.4(S - 35) + 0.017D \qquad (2)$$

where C is the sound speed in m s^{-1}, t = temperature in °C, S = salinity in PSU, and D = depth in meters (which represents the pressure effect). In the upper layers, where temperature varies most, sound speed is chiefly determined by this parameter, but in deep water (below about 2000 m) depth (or pressure) is the dominant factor (Urick, 1983).

Sound can travel long distances in the sea by some form of ducted propagation. When sound travels in a duct, or sound channel, it is prevented from spreading in all directions, and remains confined between the boundaries of this sound channel. (Urick, 1983)

In terms of the sound speed profile (sound speed versus depth), the upper and lower limits of the sound channel are defined by two depths of equal maximum speed in the profile between which a speed minimum exists. This speed minimum causes the sea to act like a kind of lens: above and below the minimum, the speed gradient continually bends the sound rays toward the depth of minimum speed. A portion of the power radiated by a source in the deep sound channel accordingly remains within the channel and encounters no acoustic losses by reflection from the surface and bottom. Because of the low transmission loss, very long ranges can be obtained from a source of moderate acoustic power output, especially when it is located near the depth of minimum speed (Urick, 1983).

RAFOS floats use the deep sound (or SOFAR) channel to determine their position as a function of time (Urick, 1983). The long ranges the acoustic transmissions must travel between

the source and the float depend on the efficiency of sound transmission in the SOFAR channel (Paquette, 1994). If a sound channel does not exist, the uncertainty of the sound paths can be a potential source of error when determining an estimate for the sound speed.

The limits of the deep sound channel are the depths AA' in the sound speed profile from Urick (1983)(Figure 3). Different ray paths from a source in the sound channel exist, depending on whether or not the sound channel extends to the sea surface or bottom. In Figure 3.a, the speed at the surface and bottom is the same. All depths in the sea lie within the sound channel, and sound is propagated via paths that are either refracted (path one) or reflected (with consequent losses) at the sea surface and bottom (path two). In Figure 3.b, the upper bound of the deep sound channel lies at the sea surface. Here, in addition to the two types of paths one and two, refracted surface-reflected (RSR) paths occur (path three) involving losses intermediate between those of paths one and two. In Figure 3.c, the sound channel is cut off by the sea bottom, and refracted bottom-reflected (RBR) paths exist (path four). The entirely refracted paths and the low transmission losses associated with these paths do not exist when the source or the receiver is outside the depth limits AA' of the sound channel (Urick, 1983).

In the Pacific, Johnson and Norris (1968) found little change in the deep sound (SOFAR) channel depth (Figure 4) and sound speed between 40° N and 40° S. A maximum mean sound speed in the sound channel of 1484 m s^{-1} was found near the equator tapering to a minimum mean sound speed in the sound channel of 1480 m s^{-1} at 40° N and 40° S. Podeszwa (1976) analyzed well over 100,000 sound speed profiles for the North Pacific Ocean producing numerous representative seasonal sound speed profiles for specific regions of the North Pacific

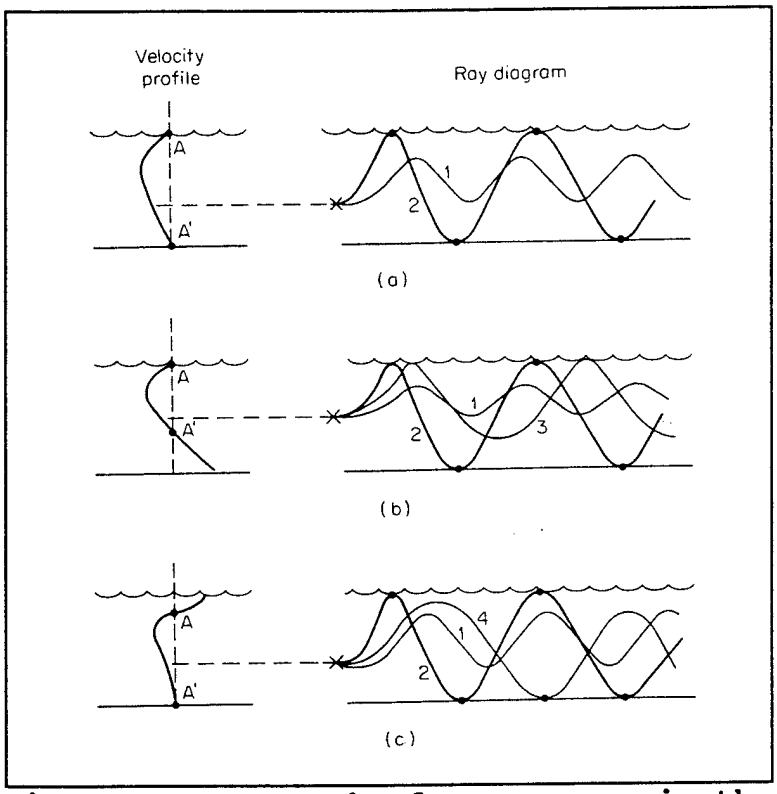

Figure 3. Ray paths for a source in the deep sound channel. In (a) the channel extends between the sea surface and bottom; in (b) and (c) it is cut off by the sea surface and by the sea bottom, respectively. [From Urick 1983].

Ocean. Though coastal profiles were not determined, as explained below, a mean value of 1481 m s^{-1} was chosen and used as a standard sound speed for this region. This value is similar to the value obtained from Figure 5.

In the shallow waters of coastal regions and on the continental shelves, the sound speed profile tends to be irregular and unpredictable due to changes in salinity and temperature occasioned by wanderings of the CC and the CUC and by the upwelling of cold mid-depth water under the influence of northwest winds (Robert G. Paquette, Personal Communication). If a sound channel does not exist, significant problems, due to sound speed and ray path variation, may exist in determining float trajectories as will be discussed later.

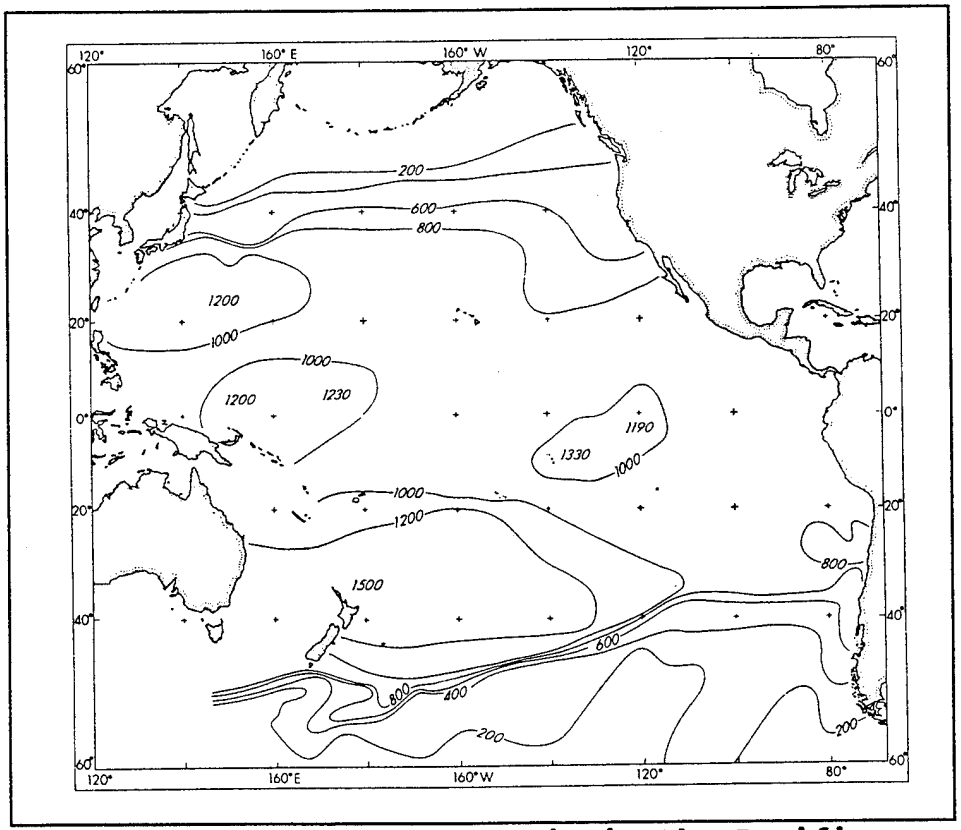

Figure 4. Depth of SOFAR Axis in the Pacific Ocean. (Contour interval 200 meters) [From Johnson and Norris 1968]

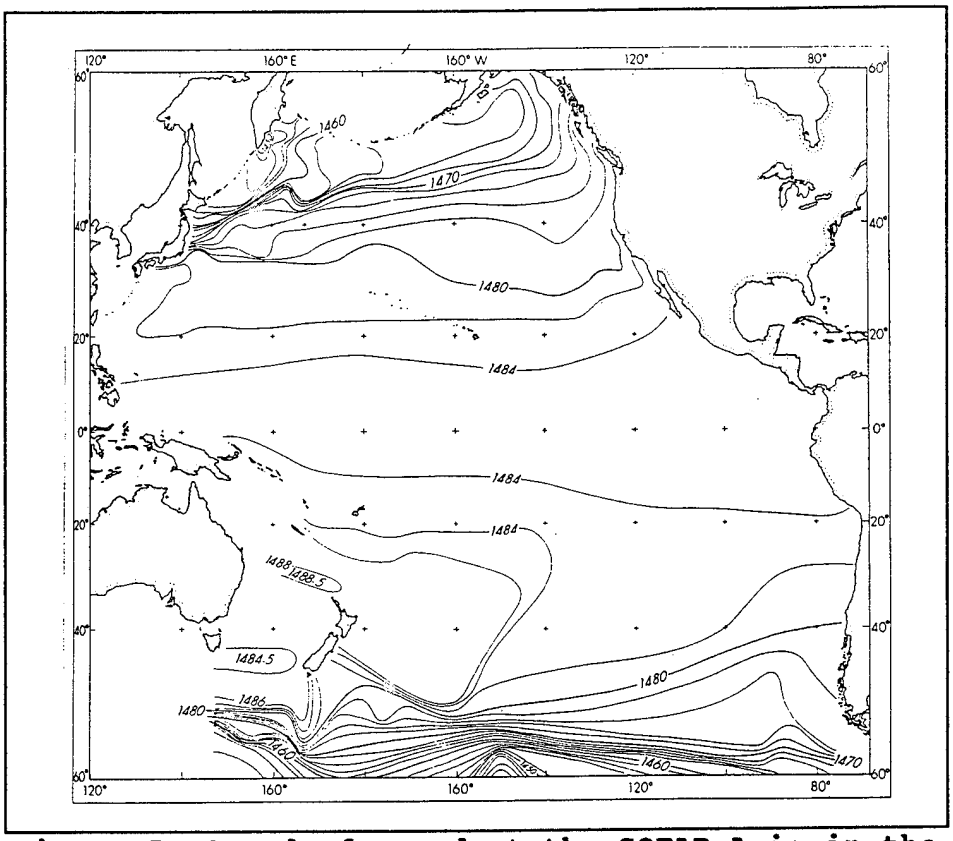

Figure 5. Speed of sound at the SOFAR Axis in the Pacific Ocean. (Contour interval 2 m/sec) [From Johnson and Norris 1968].

III. DATA COLLECTION AND PROCESSING

A. DATA COLLECTION: THE RAFOS SYSTEM

The RAFOS float is a small, neutrally buoyant, subsurface drifter, which, like its "cousin" the SOFAR float, uses the timing of sound signals in the SOFAR channel to determine its position over large regions as a function of time. Whereas the SOFAR float transmits to moored receivers, the RAFOS float listens for accurately timed signals from moored sound sources to determine its position. The acoustic signal detection and storage of data are all handled by a CMOS microprocessor in the float. The data are recovered at the end of its mission when the float surfaces and telemeters its memory contents via System ARGOS, a satellite-borne platform location and data collection system (Rossby et al., 1986).

The RAFOS float measures temperature, pressure, and times of arrival (TOA) of the acoustic signals from the moored sound sources. Temperature is obtained from a standard oceanographic thermistor that has an accuracy within 0.1° C. Pressure is measured with a strain gauge pressure transducer. The accuracy of the transducer is ±0.5% of full range, thus the expected accuracy in this study is a minimum of ±5 dbar. (Rossby et al., 1986)

Tracking information is obtained by measuring at the RAFOS float the TOA of acoustic signals from the moored sound sources. The acoustic signal consists of an 80 second continuous wave (CW) pulse centered near either 260 Hz or 400 Hz. The frequency of the pulse increases linearly 1.523 Hz throughout the 80 second broadcast. The RAFOS float contains an internal clock which, ideally, maintains synchronization with the schedule of the moored sound sources (Rossby et al., 1986). A listening window opens at a predetermined interval

for each source and TOA is determined by correlating the hydrophone signal with a stored representation in the float.

There are numerous steps involved in preparing a RAFOS float to be deployed on an operational mission. Rossby and Dorson (1983) and the RAFOS Group (1994) both discuss in detail the steps to be followed for successful deployment of a RAFOS float. First and foremost, the mission characteristics should be determined, such as how long the float will be deployed and how often data should be collected. Subsequent steps will be programming the onboard ROMs, setting the real time clock, performing temperature and pressure calibrations and completing a thorough electrical checkout of the circuitry. Once these steps are complete, the float is sealed, then ballasted for the desired target depth of the mission. (RAFOS Group, 1994)

The object of ballasting a RAFOS float is to make it neutrally buoyant at a desired depth in the ocean. This is accomplished by adjusting the density of the float at the target depth to the density of the seawater at the same depth. The volume and weight of the float are first measured at atmospheric pressure. The density is then determined at the target pressure, but using fresh, ideally de-ionized, water of a different (other than target depth) temperature. The final adjustment to the weight is made by determining the additional weight needed to compensate for: a) the difference in density between the fresh water and the target seawater; b) temperature contraction; and c) pressure compression. The calculations to do these corrections are done starting with the volume and weight of each of the components of the system (i.e., RAFOS float and drop weight). These weight calculations are usually within 0.1 grams. (RAFOS Group, 1994)

The target depth for each float in this study was 275 m, but actual depths were substantially deeper (Table 1). This depth error can be caused by improper ballasting or leakage

into the hollow ballast weight. Improper ballasting can arise from a number of sources, such as poor knowledge of the in situ density or uncertainty in the density of the water in the ballast tank. Both improper ballasting and leakage appear to have been the reason that these tomography floats settled to a level deeper than intended.

The ballasting tank used to ballast these floats was filled with city tap water and not distilled water. The density of this water was estimated by measuring the submerged weight of a five foot piece of RAFOS glass having a density slightly greater than water. The equation of state was then run regressively to estimate the salinity that would give the calculated density. For this batch of floats, the estimated salinity was 0.9 PSU. It appears this value was low, and a more appropriate value should have been between 1.05 PSU and 1.1 PSU. This change would account for much of the difference between the target and actual depths, however, because the floats did not all have similar depth errors, it is believed that leakage into the hollow ballast weights was a factor as well in these depth discrepancies. These discrepancies together with the float parameters are shown in Table 1.

In a "typical" mission, the RAFOS float listens for three different sound sources every eight hours with a 20 minute offset for each source. The TOAs for the two best correlating signals heard in a usually 820-second window, corresponding to a maximum range of 1230 km, are stored for each source. Pressure and temperature are measured at the end of each complete cycle (Rossby et al., 1986). In this study, acoustic signals were received once per hour, with a twenty minute offset for each source; temperature and pressure were recorded at the end of each cycle. At 9, 29, and 49 minutes past

FLOAT NAME NPS # ARGOS PTT	LAUNCHED TIME/DATE POSITION	DEPTH (m) TARGET/ACTUAL	SURFACED TIME/DATE POSITION
Mickelinc NPS #21 22481	0522Z/19May94 36° 35.47′ N 122° 35.36′ W	275/380	2054Z/10Jun94 38° 20.70′ N 124° 05.82′ W
Arata NPS #22 22480	0302Z/19May94 36° 31.26′ N 122° 48.50′ W	275/604	2054Z/10Jun94 37° 39.66′ N 124° 09.42′ W
Feller NPS #24 22479	2347Z/17May94 36° 20.26′ N 123° 01.24′ W	275/573	2154Z/09Jun94 37° 29.28′N 123° 52.32′ W
Steiner NPS #27 8840	0045Z/19May94 36° 40.33′ N 123° 0.53′W	275/Unknown	2054Z/10Jun94 38° 3.54′ N 124° 7.68′ W
Steger NPS #30 4143	0226Z/18May94 36° 29.98′ N 123° 00.06′ W	275/302	0054Z/10Jun94 37° 28.32′ N 124° 18.78′ W

Table 1. Float Parameters.

the hour, the float would open a 300-second window to listen for the acoustic signal from each of the three sound sources, respectively. The shorter windows during this mission were necessitated by higher frequency of sampling. These floats also used a CW pulse centered at 400 Hz vice 260 Hz to avoid interference with float-tracking in progress using the lower frequency.

At mission end the CPU activates a release circuit which drops the ballast weight to return the float to the surface. Thirty minutes after release the ARGOS transmitter is turned on. The format for the radio transmission is structured to

conform to the requirements of the ARGOS System. The float transmits the entire contents of its memory, in quasi-random order, to allow the satellite to receive the full data set. A satellite pass is within range for less than 15 minutes, so a number of orbits are required to successfully transfer the complete data set. Typically, at least three days are required to complete the entire transfer of data (Rossby et al., 1986). Previous experience suggest that at least 30% of the data are obtained within one day, and more than 90% are obtained after three days (Rossby and Dorson, 1983). Each message received is identified by an ARGOS message number and contains a checksum. From the concatenated ARGOS messages, the shorter RAFOS messages must be extracted. The floats continue to transmit their memory contents for 150 complete cycles, then the transmitter shuts down; a period which took about 2.5 months.

B. ERROR SOURCES

Once the raw data are received and throughout the subsequent processing cycle, there is great potential for inaccurate final solutions of the float trajectory unless numerous causes of errors are considered and minimized. The long-term and constant (systematic) errors affect general position accuracy, whereas the short-term quasi-random errors affect the ability to extract high frequency float motion information.

Systematic errors are those which follow some law by which they can be predicted. An error which can be predicted can be eliminated, or compensation can be made for it. (Bowditch, 1984) Examples of systematic errors include, but are not limited to: variations of sound speed and float/source clock errors. Random errors are chance errors, unpredictable in magnitude or sign. They are governed by the laws of probability (Bowditch, 1984). Examples of random errors

include non-constant sound speed propagation modes, including multipath, the float correlator and all other noise of unknown origin (ambient). These errors can also be magnified, depending on the configuration of the source to float geometry. All of these errors and their magnification will be discussed further.

1. Sound Speed

As previously discussed, the speed of sound in the ocean varies with temperature, salinity and pressure. The sound speed versus depth profiles (Figure 6) show that no significant sound channel appears to exist during the experiment period. Because the CTD records do not extend to the ocean bottom, a deeper sound channel may in fact exist that is deeper than what is expected in the region of interest for this study. It must be kept in mind, however, that the entire acoustic structure of this region cannot necessarily be depicted from only three CTD casts. Because of the close proximity to the shore, the irregular variability of the sound speed hinders the determination of an actual sound speed. For this same reason, Johnson and Norris (1968) and Podeszwa (1976) came to no conclusions concerning a sound channel in these shallow coastal waters. In the processing programs, discussed by Paquette (1994), a single sound speed of 1481 m s^{-1} is used throughout the processing. This value is considered to be the average sound speed at the axis of the SOFAR Channel near this region of the Pacific as determined by Johnson and Norris (1968). This may be an inappropriate value for sound speed considering the existence of a sound channel cannot be confirmed.

Because the speed of sound varies with depth, it is difficult, and incorrect, to assume a single sound speed exists between the source and float. At Source One, the sound

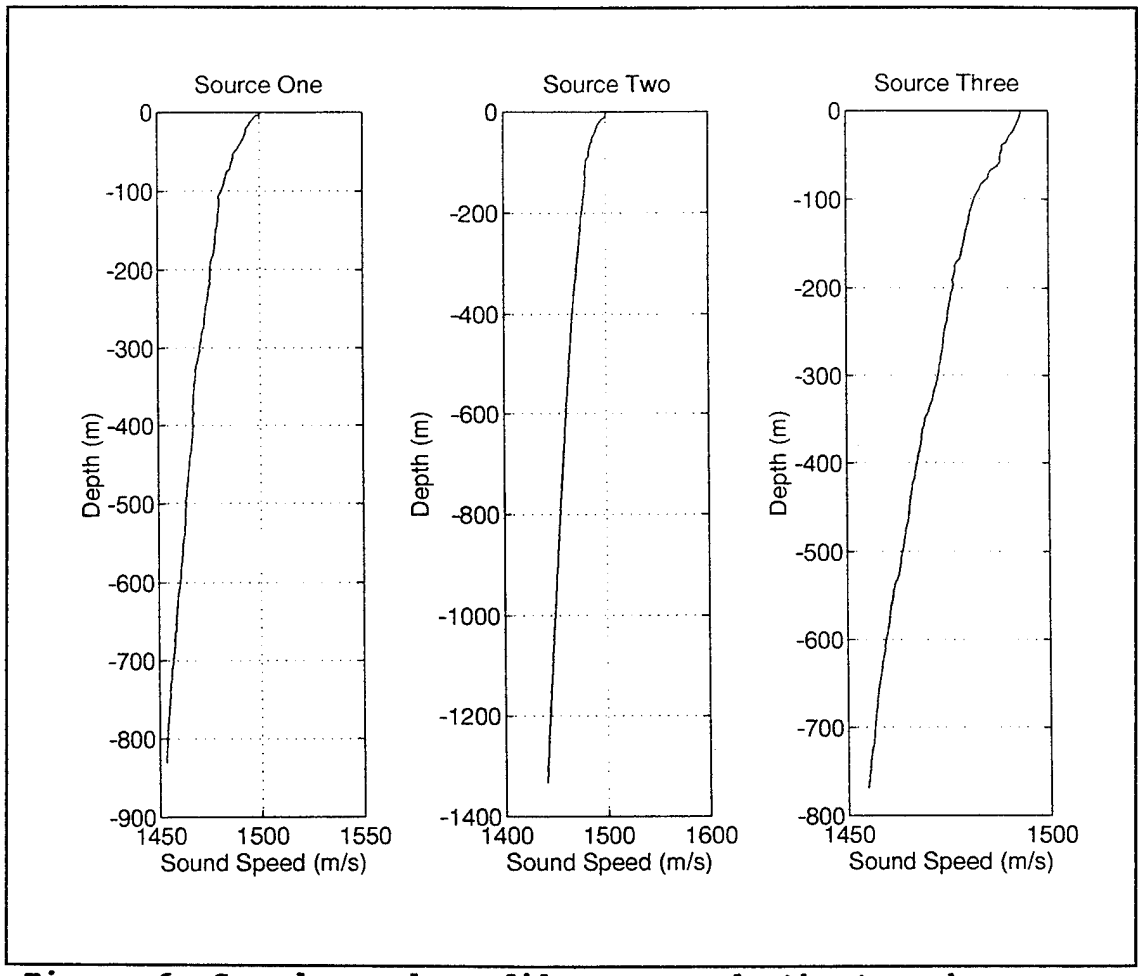

Figure 6. Sound speed profile versus depth at each source. a) Source One, b)Source Two, c)Source Three.

speed at the bottom (832 m) is approximately 1453 m s^{-1} and at the surface it is 1500 m s^{-1}. Assuming the depth range of propagation is the entire water column, the depth averaged sound speed in the entire water column at this location would be approximately 1477 m s^{-1}, which could be a good first approximation for the actual sound speed. It must be kept in mind, however, that because of the variance in sound speed from the ocean bottom to the surface, sound rays will not remain at a constant speed throughout their path. An integrated sound speed for this water column is 1468 m s^{-1}. Because anomalous sound speed profiles may occur throughout the ray path due to this location's close proximity to the coast, the exact sound speed cannot be determined with great accuracy. The first approximation equates to a sound speed difference at a minimum of 4 m s^{-1}. Using the standard 1481 m s^{-1}, that is equal to a potential 0.5 km error at 200 km. Similarly, at Source Two and Source Three, potential errors exist on the order of 1.5 km and 1.0 km, respectively. This difference is due mainly to the different depths of each source and float.

Because the sound sources in this study are omnidirectional, sound rays from an infinite number of different angles are emitted from the source, and thus can expect many sound paths between the source and the floats, i.e., the types of ray paths cannot be determined with any certainty. This is called multipath propagation. Multipath propagation causes fluctuations in phase and amplitude at a single receiver, such as a RAFOS float. Multipaths also cause signal distortion because the travel times along different paths are different, which can lead to different TOAs for the same sweep from the source (Urick, 1983). The errors caused by multipaths are extremely difficult to estimate, but are relatively insignificant at the short distances in this mission.

2. Interval Between Launch and First Fix

A potential processing induced error may occur when trying to navigate a float to the launch position, as is the case in the traditional two-source (ARTRK) method discussed in Section III.C. Once a float is launched, a maximum of just over one hour can be expected to elapse before the first acoustic fix is obtained from the sound sources. This results in a potential distance error of approximately 0.5 km for a current speed of 10 cm s^{-1}. Table 2 displays the interval times between launch and the first fix for each float.

FLOAT ID	LAUNCH TIME/DATE	FIRST FIX TIME/DATE	ΔT (Minutes)	POTENTIAL ERROR (KM)
NPS #21	0522Z 19 May 94	0649Z 19 May 94	87	0.5
NPS #22	0302Z 19 May 94	0349Z 19 May 94	47	0.3
NPS #24	2347Z 17 May 94	0049Z 18 May 94	62	0.4
NPS #30	0226Z 18 May 94	0349Z 18 May 94	83	0.5

Table 2. Interval between launch and first fix.

3. Interval Between Last Fix and First ARGOS Fix

Another potential processing induced error is the time interval between the last submerged fix from the sound sources and the first ARGOS Satellite fix at the surface, as is also done in the traditional two-source (ARTRK) solution discussed in III.C. The time difference between these two fixes can be anywhere from three to six hours. Table 3 summarizes the

times of the last submerged fix and the first ARGOS hit (the time the satellite first sees the float).

Once the float is on the surface and detected by ARGOS, it may take from one to two hours for the satellite to get an accurate fix on the float. Table 4 summarizes the time it took ARGOS to obtain a fix for each float and the subsequent total time between the last submerged fix and the first surface fix.

FLOAT ID	LAST SUBMERGED FIX	FIRST ARGOS HIT	ΔT (Hours)
NPS #21	19:09:12Z 10 Jun 94	22:05:52Z 10 Jun 94	2.94
NPS #22	19:09:12Z 10 Jun 94	23:40:57Z 10 Jun 94	4.53
NPS #24	20:09:48Z 9 Jun 94	22:15:48Z 9 Jun 94	2.10
NPS #30	23:09:36Z 9 Jun 94	01:38:48Z 10 Jun 94	2.49

Table 3. Time difference between last submerged fix and the first ARGOS hit.

FLOAT ID	ELAPSED TIME FOR ARGOS FIX (Hours)	ΔT FROM TABLE 4. (Hours)	TOTAL TIME BETWEEN FIXES (Hours)
NPS #21	1.66	2.94	4.60
NPS #22	1.68	4.53	6.21
NPS #24	1.66	2.10	3.76
NPS #30	0.71	2.49	3.20

Table 4. Total time between submerged and surface fixes.

From these measurements, the delay between the last acoustic cycle and the first ARGOS fix varies between 3.20 and 6.21 hours. Exactly 30 minutes after the ballast weight is released, the float begins to transmit (Rossby and Dorson, 1983). If we assume that the ballast weight is released immediately after the last acoustic cycle, and the float takes the complete 30 minutes to rise to the surface (depending on operational depth of the float), then the floats could have been drifting on the surface anywhere from 2.78 to 5.64 hours prior to the first ARGOS fix. Surface drift data were recovered from ARGOS for each float, and Table 5 summarizes the average surface drift and the potential distance between the surfacing and ARGOS first fix positions.

FLOAT ID	AVERAGE SURFACE CURRENT (CM S^{-1})	DISTANCE BETWEEN SURFACING AND FIRST ARGOS FIX (KM)
NPS #21	18.5	2.73
NPS #22	24.9	5.12
NPS #24	12.6	1.48
NPS #30	17.2	1.67

Table 5. Potential distance between surface position and first ARGOS fix.

4. Other Sources of Error

The previously mentioned error sources can be classified as significant sources of error. There also exists other sources of error such as source and float clock drift, the TOA Correlator, and ambient noise.

In this experiment, the source clock drifts were available because the sound sources were recovered upon

completion of the experiment. The clock readings at the end of the mission were compared with the values obtained prior to launch and a source clock drift was determined for each source as summarized in Table 6. These values are relatively small and considered insignificant, however, over a much greater length of time, these values could become very significant.

SOURCE	CLOCK DRIFT (msec/day)
1	0.622
2	2.233
3	-1.16

Table 6. Measured source clock drift.

Because RAFOS floats are usually not recovered once they surface (they were not recovered in this experiment), it is not possible to determine an accurate drift of the float clock. NPS maintains an operational RAFOS Board which is connected to hydrophones at the Point Sur Underwater Acoustic Observatory, California. Typical clock drift experienced here over a similar time period is on the order of 0.06605 sec day^{-1}. If we assume this to be the standard drift for each float, the error potential is on the order of 100 m at mission end, which is relatively small, and therefore insignificant. Again, if this drift was taken over a much greater length of time, the error potential could become a factor.

Tracking information is obtained by detecting at the RAFOS floats sound signals from the moored sound sources and comparing them to ideal signals stored in float memory. The three best correlated TOAs are determined by listening to numerous consecutive 80 second windows, separated by one

decisecond, and comparing the received signals to the ideal signal. The float then keeps the two best correlations. The correlator has an inherent minimum error equating to about ±0.3 seconds, potentially producing an error of about 0.4 km. (Pierre Tilliet, Personal Communication)

Ambient noise is the remaining noise in the sea after all identifiable noise sources are accounted for. Ambient noise has different characteristics at different frequencies. Because of this, it follows that the noise must be due to a variety of different sources. Since these RAFOS Floats operate at 400 Hz, the dominant contributor to ambient noise at this frequency would be ship traffic. Sources of ambient noise can contribute to degradation of the received sound signal at the float and are a potential cause of error, which is difficult to estimate with any certainty. (Urick, 1983)

5. Total Error

An estimated total system error at the launch and surface points can be determined by calculating a root mean square (RMS) of all the sources of error mentioned above. Equation 3 shows the components of the total error (ϵ_T).

$$\epsilon_T = [(\epsilon_{SV})^2 + (\epsilon_{RP})^2 + (\epsilon_{LI})^2 + (\epsilon_{SI})^2 + (\epsilon_{SC})^2 + (\epsilon_{FC})^2 + (\epsilon_{TC})^2 + (\epsilon_{AN})^2]^{1/2} \quad (3)$$

where each source of error is as follows: ϵ_{SV} = errors due to uncertainty in the sound speed profile, ϵ_{RP} = errors due to uncertainty in ray paths, ϵ_{LI} = errors due to launch interval, ϵ_{SI} = errors due to surface interval, ϵ_{SC} = errors due to source clock error, ϵ_{FC} = errors due to float clock error, ϵ_{TC} = inherent errors in the TOA correlator, and ϵ_{AN} = errors due to degradation of the signal by ambient noise. Table 7 summarizes this total RMS system error in the navigation of each float at mission beginning (first

submerged fix) and end (last submerged fix). With increasing distance from the sources, this error will increase.

FLOAT ID	INITIAL RMS ERROR (KM)	FINAL RMS ERROR (KM)
NPS #21	1.93	3.34
NPS #22	1.91	5.47
NPS #24	1.92	2.43
NPS #30	1.93	2.55

Table 7. Estimated RMS Error at launch and surface points.

These errors can be compensated for if an accurate estimation is made of systematic and random errors. If we assume the floats travel at their combined average speed of 9.5 cm s^{-1}, in one hour they will only travel 0.34 km. This distance is less than the maximum error presented in Table 7, which shows that unless the errors can be accounted for, this higher frequency sampling may not be beneficial when compared to traditional sampling periods.

Since the errors can be compensated for in most situations, the higher frequency sampling techniques of these floats can provide a good record of float trajectories when sufficient data are available; however, high-frequency current changes may not be detectable if high-frequency random errors cannot be accounted for.

6. Source to Float Geometry

A major factor in determining an accurate navigational solution is the physical geometry of the sound sources and the position of the float. The triangle formed by the two sources and the float in the two-source tracking method and the configuration between all three sources and the float in the three-source method must be examined. If the float passes across the baseline between two sources, the navigation of the float at that point generally will be adversely affected and often will fail entirely. A factor, referred to as the Dilution of Precision (DOP), links the accuracy of the range information from each source to the accuracy of the final navigational solution (Eipp, 1995).

The DOP can be calculated by taking distance vectors between each source and an estimated first guess position to form unit vectors. These unit vectors are summed and combined to form a matrix, which is called the Partials Matrix (H). H contains information on how the errors in range are distributed among the solution components (x and y) at a specific point. The DOP is calculated using the following equation:

$$DOP = \sqrt{Trace(H^T H)^{-1}} \qquad (4)$$

where Trace $(H^T H)^{-1}$ is the sum of the diagonal elements of $(H^T H)^{-1}$.

The DOP gives the multiplication factor of the estimated distance measurement error for the estimation of total position and time errors (Forsell, 1991). The closer the DOP is to one, the better the solution you will obtain, and subsequently, the least amount of error due to source geometry. Figure 7 depicts a DOP Contour Plot for three sound sources of the mission region in grid coordinates, with the origin located arbitrarily at 35°N 125°W. Figure 8 depicts an

example of a DOP Contour Plot for two sound sources (Sources Two and Three in this case).

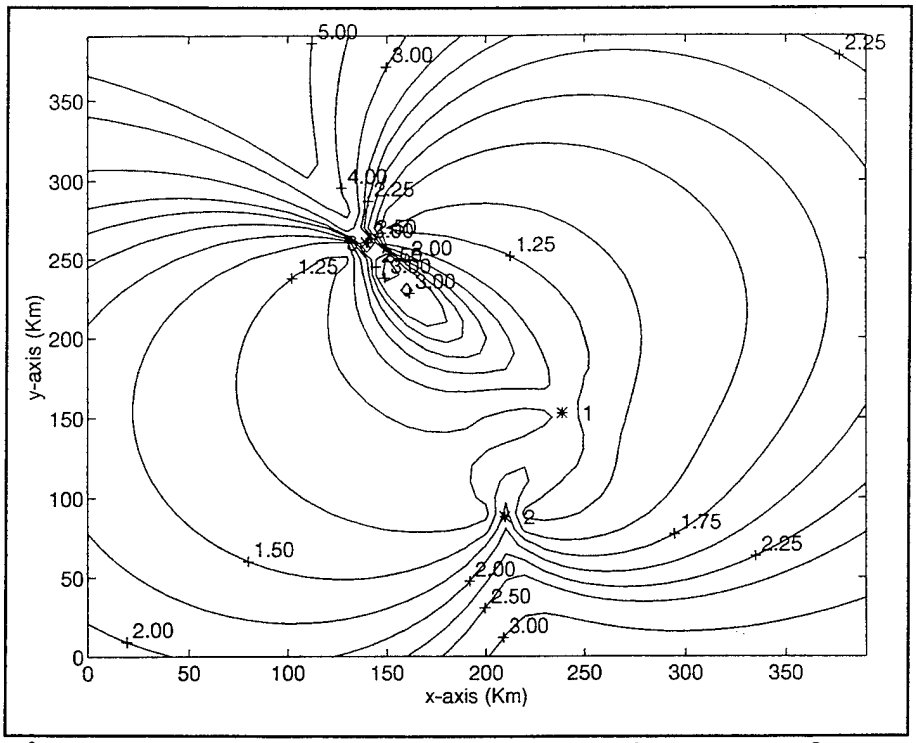

Figure 7. DOP Contour Plot for three sound sources.

A good example of how geometry can affect a navigational solution is shown in Figure 9. Here we can see that the launch position is directly on the baseline between Source Two and Source Three. Referring to Figure 8, we can see that the DOP in this region is on the order of 20, which corresponds to an extremely poor geometry for two sources. Because of the location of the launch for NPS #30, it is extremely difficult, to obtain an accurate solution for the float track at the launch position. Another way to view this concept is that a small systematic error will have little effect when a float is near the sources, but the farther away the float gets from the sources, the error will grow.

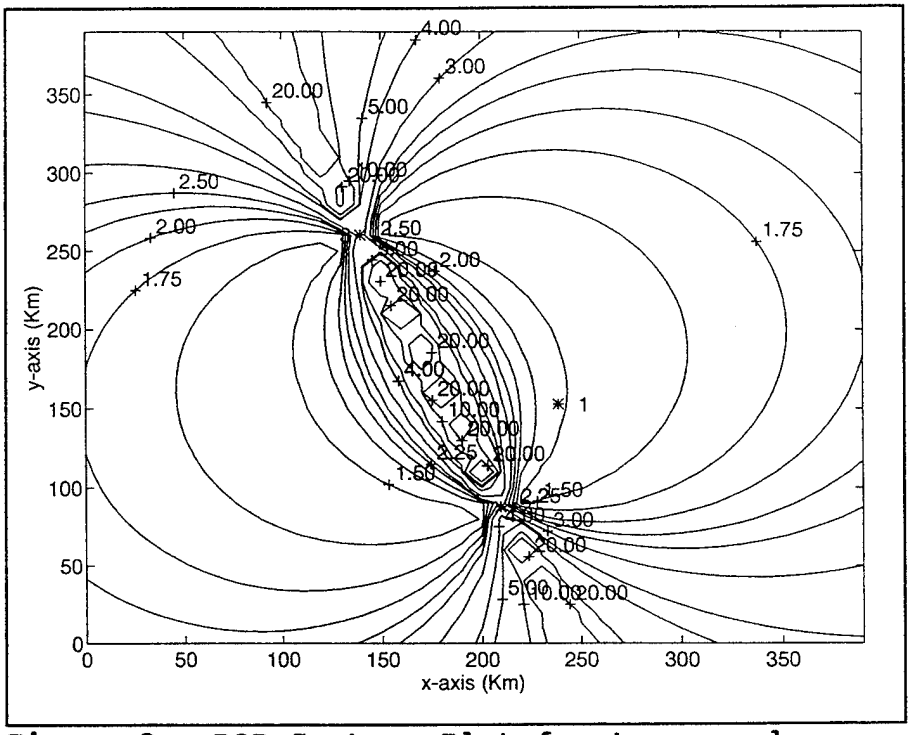

Figure 8. DOP Contour Plot for two sound sources. (Sources Two and Three).

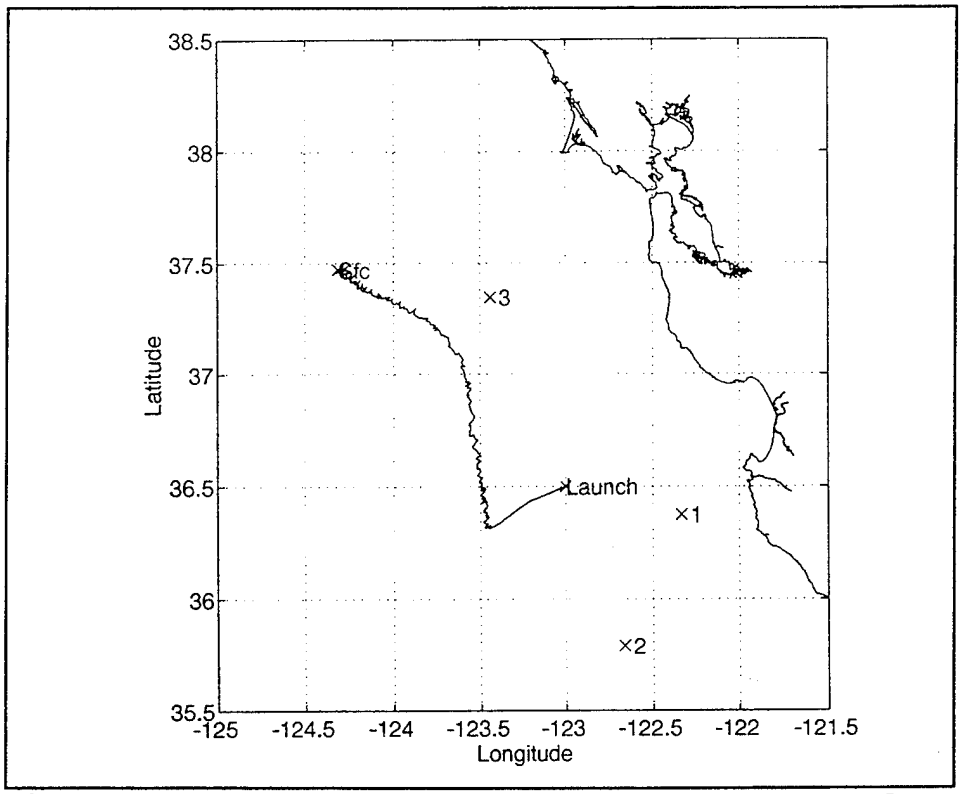

Figure 9. Poor geometry between Sources Two and Three for launch position of NPS #30.

C. DATA PROCESSING

The first step in data processing is to group the ARGOS data messages according to float and to check that each message has not been corrupted during transmission. On calm days at sea, approximately 90% of the data transfers are found to be error-free, however, in severe weather, this percentage can drop to about 50% (Rossby et al., 1986). The traditional SOFAR/RAFOS Processing Programs (Paquette, 1994) such as SETUP, DECIDE, and ARTOA are used upon completion of gathering a raw data file for each float to extract a data file in

record sequential order which contains temperature and pressure in decimal integer form and a TOA from each moored sound source.

In the processing program ARTOA, correlation heights (*korght*) of the two best correlated TOAs from each sound source are converted into quality numbers. Values of *korght* > 60, 60 > *korght* > 50, 50 > *korght* > 40, *and korght* ≤ 40 are transformed into quality numbers 3,2,1,0 respectively. The main editor of this particular program allows the TOA to be edited and provides a rather clever graphic editor that plots the two best correlated TOAs from each source (one source at a time) as a symbol in a left-right position on the screen corresponding to the TOA. The first TOA is plotted with the quality number, mentioned above, as the symbol. The second TOA of the source is plotted with the letters a, b, c, and d corresponding to the quality numbers 0, 1, 2, and 3. If the plotting parameters are chosen appropriately, a curving graph extending from top to bottom in proportion to record number and curving back and forth from left to right in proportion to TOA (Figure 10) is obtained. It is easy to see if TOAs are missing or out of place and if the second TOA from a source is more consistent than the first. For example, in Figure 10, the record number and two TOAs are listed at the left. Clearly there is a pattern present on the right side, and TOAs not falling on this line are obvious. The objective of this

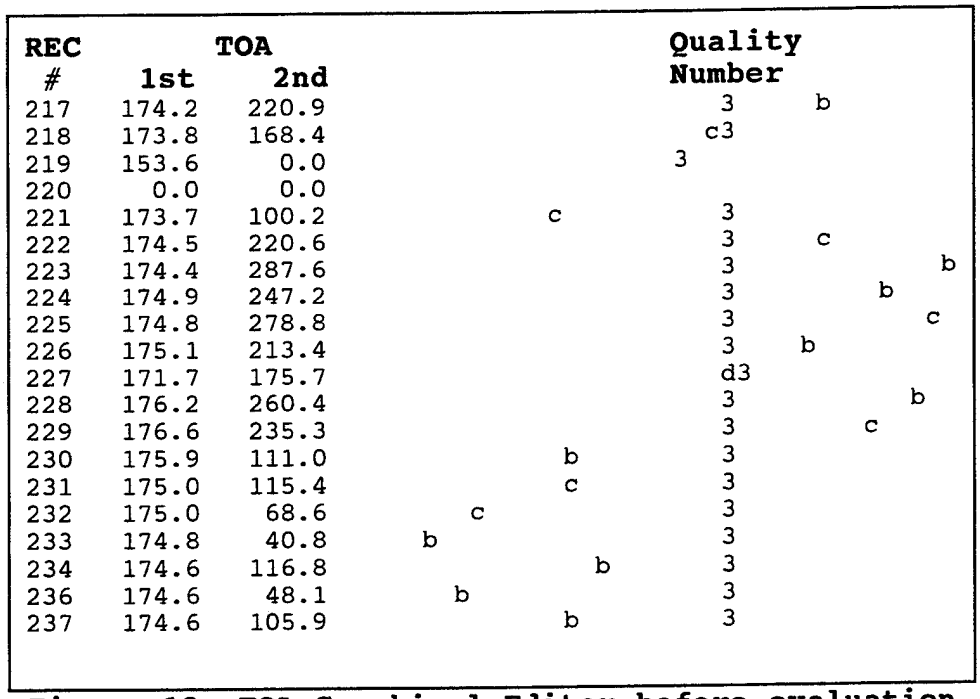

Figure 10. TOA Graphical Editor before evaluation (NPS #24, Source One).

editing step, therefore is to zero (kill) the obviously incorrect TOA of each pair or to zero both if both are inconsistent (Paquette, 1994). Once the TOA editing is complete, the resultant graph described in Figure 10 above will become similar to that in Figure 11.

REC #	TOA 1st	TOA 2nd	Quality Number
217	174.2	0.0	3
218	173.8	0.0	3
219	0.0	0.0	
220	0.0	0.0	
221	173.7	0.0	3
222	174.5	0.0	3
223	174.4	0.0	3
224	174.9	0.0	3
225	174.8	0.0	3
226	175.1	0.0	3
227	0.0	175.7	d
228	176.2	0.0	3
229	176.6	0.0	3
230	175.9	0.0	3
231	175.0	0.0	3
232	175.0	0.0	3
233	174.8	0.0	3
234	174.6	0.0	3
235	174.2	0.0	3
236	174.6	0.0	3
237	174.6	0.0	3

Figure 11. TOA Graphical Editor after evaluation (NPS #24, Source One).

Once the final data file is complete, which consists of time, temperature, pressure and a TOA from each source, a trajectory of the float throughout the mission can be determined. This is not a simple task, as the systematic and random errors exist in the TOA records. If not accounted for, the resultant solutions will be difficult to obtain. In equation form, a TOA is basically

$$\rho_m = \rho_0 + \epsilon_T \tag{5}$$

where ρ_m is the measured TOA, ρ_0 is the true TOA, and ϵ_T is the total error from Equation 3. ρ_m can be expanded as follows

$$\rho_m = (t_R - t_S)C = (\boldsymbol{X}_R - \boldsymbol{X}_S) \tag{6}$$

where t_R is the measured time of receipt of the acoustic signal at the float, t_S is the measure time of transmission of the acoustic signal from the source, C is some average sound speed, and $\mathbf{X_R}$ and $\mathbf{X_S}$ are position vectors for the float and source, respectively.

Due to clock drifts in the float and sources and other sources impeding the receipt of the acoustic signal, the actual times, t_{RO} and t_{SO}, can be related to t_R and t_S as follows

$$\begin{aligned} t_R &= t_{RO} + \tau_R \\ t_S &= t_{SO} + \tau_S \end{aligned} \tag{7}$$

where t_{RO} and t_{SO} are the actual times of the acoustic signal receipt and transmission respectively, and τ_R and τ_S are some drift of the time at the float and source, respectively, attributed to ϵ_T.

From Equation 6, $\mathbf{X_R}$ and $\mathbf{X_S}$ can be partitioned into their three components as follows

$$(\mathbf{X_R} - \mathbf{X_S}) = [(x_R - x_S)^2 + (y_R - y_S)^2 + (z_R - z_S)^2]^{1/2} \tag{8}$$

where x_R, x_S, y_R, y_S are the x and y (longitude and latitude) components of $\mathbf{X_R}$ and $\mathbf{X_S}$, and z_R and z_S are the depths of the float and source, respectively.

To determine a float trajectory (a series of x_R and y_R), the known and unknown variables must be separated. The known variables are x_S and y_S (source positions), z_R (depth of floats from pressure records), z_S (depth of sources), the measured TOAs, or t_R and t_S (measured times of acoustic signal receipt and transmission), and τ_S (from Table 6). The unknown variables are x_R and y_R (the float position) and τ_R (the drift seen in the float clock due to the total error minus the source drift ($\epsilon_T - \epsilon_{SC}$).

To determine a solution (x_R and y_R), a value for τ_R must be estimated to achieve a plausible trajectory. Two techniques were used to obtain a navigational solution for each float. The traditional SOFAR/RAFOS two-source solution (ARTRK) was obtained by using the ARTRK Program (Paquette 1994). This method does not take into account z_s, and a value for τ_R is determined as described below. A three-source solution is obtained using an ordinary mean least square (OMLS) technique similar to that used by GPS (Clynch 1995). With an ARTRK solution, there is no formal way to estimate either the random or systematic errors. With three ARTRK solutions, the random and systematic errors can be adjusted by trial and error to collapse each solution to similar tracks, but this can be time consuming and depends on human skill. With an OMLS solution, an estimate of the random and systematic errors can be mathematically estimated and used as a correction to an ARTRK solution. These resultant solutions can then be compared with the initial solutions to assist in determining a correct float trajectory.

1. Two-Source (ARTRK) Solution

In the final processing program, ARTRK (Paquette, 1994), a synthetic correction must be estimated to compensate for systematic errors. The apparent clock offsets and drifts are estimated by forcing the first subsurface fix to the launch point and the last subsurface fix to the first ARGOS position, as introduced in Section III.B. This is accomplished by taking the TOAs from the first fix and comparing them to what the TOAs should be at the launch position (assuming sound speed equals 1481 m s^{-1}). The difference is the initial offset. At the end of the float track, the TOAs from the last fix are compared to what the TOAs should be at the first ARGOS position to determine a final offset. From the initial and final offsets, a drift can be calculated for the entire track.

This not only compensates for float and source offsets and drifts (systematic errors), but also for sound speed and other unknown errors (random errors), which are apportioned over the drift tracks. When trying to navigate the trajectory to the launch and surface positions, the additional interval error between launch and first fix, and last subsurface fix and first ARGOS fix must be taken into account. TOAs are then interpolated and a latitude and longitude for each fix is calculated.

The float positions for each fix are actually determined by estimating a range from each source from the measured TOA and finding the position that is separated from each source by the determined distance respectively. This solution is then compared to the solutions from the remaining two source pairs, and a final position is estimated. If all three pairs of sources produce a fix at the same point, then no error is present, but if they do not fall on the same spot, error (systematic and random) does exist, and this error can be estimated for each source by the method described above. (Paquette, 1994)

The fix determined by the intersection of one pair of source ranges in general can be inconsistent with a fix determined by the intersection of a second pair of source ranges. Since the inconsistency will be due to errors, the third (redundant) range measurement from the third source can be used to estimate the total error, which is minimized to all three ranges. If the estimate is correct, the three lines of position from each source will intersect at a common point. (Bowditch, 1984) The estimate of error determined from this method is useable, and good trajectories are usually obtained; making it a practical method, however, it is believed that if this error can be determined mathematically, another set of trajectories will be available to assist in determining which specific trajectory is the most probable one.

2. Three-Source (OMLS) Solution

Forsell (1991) and Clynch (1995) discuss the details of obtaining an OMLS navigational solution using all three sound sources instead of just three pairs of two sound sources. This method is often called the Rho-Rho mode. This OMLS solution is a well established surveying technique which uses multiple measurements to estimate and minimize errors. This technique uses a combination of range measurements (TOAs) from fixed reference stations (sound sources) and an estimated noise (random error) to produce a series of iterations converging on a solution (position) which minimizes and provides a value for the systematic error.

This method requires an initial error estimate (random errors) for each measurement to know how to weight the ranges. This is approximated by fitting a polynomial curve to a plot of TOAs versus time from each source (Figure 12). The error is then estimated to be the root mean square of the sums of the differences between the observed TOAs and the polynomial. This value is used to flag and remove outlying TOAs (TOAs outside this range from the polynomial)(Figure 13). The estimate for random errors for these floats was calculated to be on the order of 0.5 seconds, or 740 m using 1481 m s^{-1}. This value and the edited TOA record (estimated ranges) are then input along with a first guess of position into the OMLS technique. This first guess of position is the launch point of the float for the first solution, and the previous solution for subsequent solutions, and its purpose is only to reduce the number of iterations required to obtain a final solution.

With three ranges, the OMLS solution can be estimated in three-dimensions (x_R, y_R, and z_R), or if one of the coordinates are known, such as depth (z_R), as is the case in this study (from pressure records), the two unknown coordinates and a value for the systematic error (τ_R) can be determined. With

the OMLS technique, the solution is determined by minimizing the total difference between the measured and estimated ranges between the source and the float. If the solution is overdetermined, the systematic error can be computed for each fix.

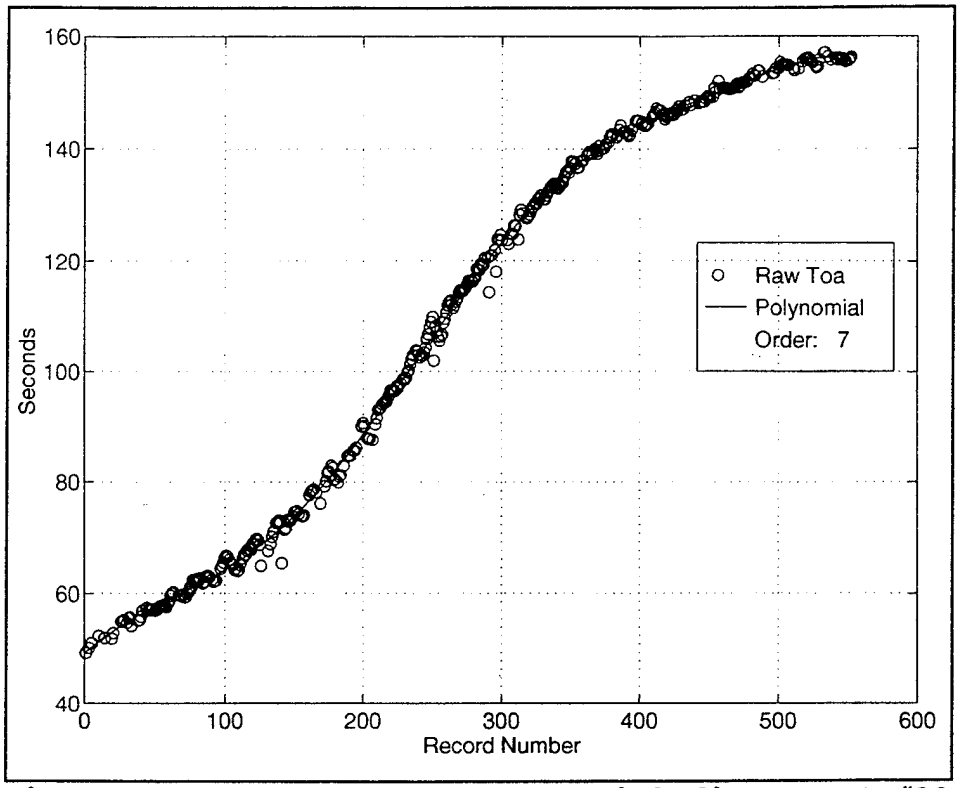

Figure 12. Seventh Order Polynomial fit to NPS #30 TOA Record from Source Two.

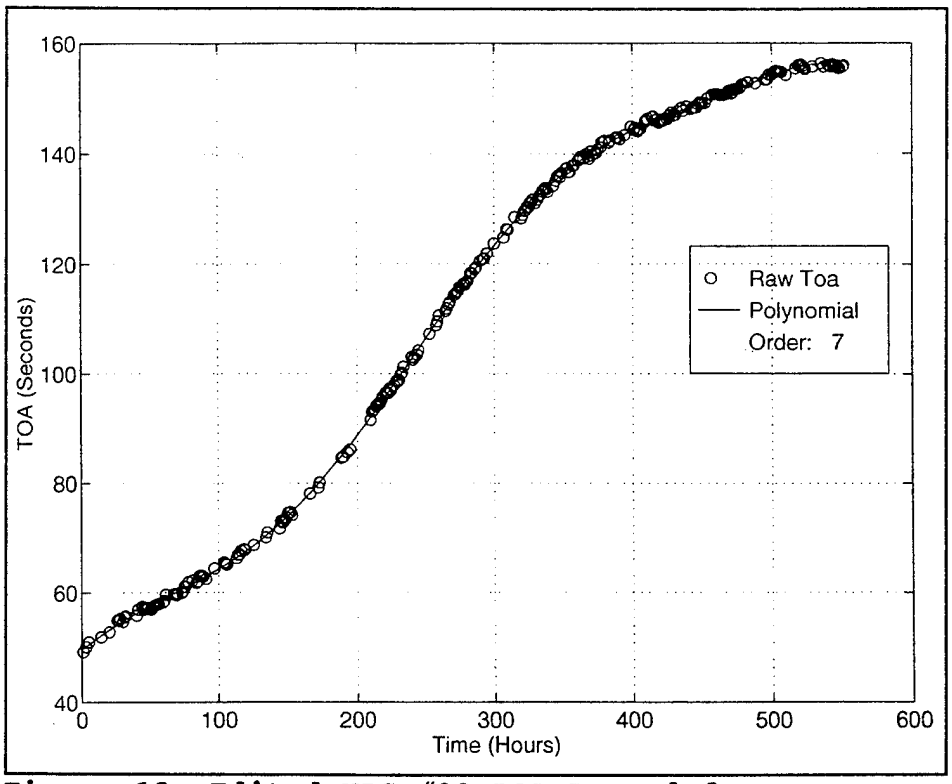

Figure 13. Edited NPS #30 TOA Record from Source Two.

Once all positions are calculated, the systematic error for each fix is plotted versus time and a line is fit to this plot (Figure 14). In this particular example, Figure 14 shows that the error "blows up" around record number 245. This corresponds to an area in the float trajectory where the DOP is increasing, thus degrading the solution. In this case, a line was fit only to the portion of the plot up to record 245 (vertical line in figure). The slope of the fitted line is a combination of source and clock drifts and the intercept is the initial offset, which could be due to either clock offset or variations of sound speed. These values for the slope and intercept are the systematic error, which is assumed linear and equally balanced between the three ranges. This correction can also be applied to the ARTRK solution to obtain a set of new solutions which can be used to assist in determining the most probable float trajectory. Table 8 displays the estimated error offsets and drifts determined for each float from the OMLS method.

FLOAT ID	DRIFT (SEC FIX^{-1})	OFFSET (SEC)
NPS #21	0.0035	-10.27
NPS #22	-0.0058	-19.65
NPS #24	0.0402	39.00
NPS #30	0.0021	-12.36

Table 8. Calculated values of systematic errors.

To view how this process is conducted, Figure 15 shows the three ARTRK solutions of NPS #30. As can be seen, each solution is different, and it is difficult to determine which one may be the "correct" trajectory (although it is obvious we can eliminate the solution from Sources Two and Three due to poor geometry as previously discussed). Figure 16 shows the OMLS solution for NPS #30. The reason this trajectory has so

many gaps in the data is because only 29% of the 552 total records recorded TOAs from all three sources. The reasons for these gaps will be discussed further in Chapter IV. With a value for the systematic error calculated from the OMLS technique in the three-source solution applied, Figure 17 depicts the three OMLS two-source solutions. Again, the solution from Sources Two and Three is obviously incorrect due to poor float to source geometry, as in the ARTRK solution. This solution actually appears to be a mirror image about the baseline between Sources Two and Three of the correct solution for this source pair. Figure 18. depicts the three ARTRK solutions with the OMLS systematic error applied. This figure looks somewhat similar to the original two-source solutions, but the solutions are a little closer together in relation to each other.

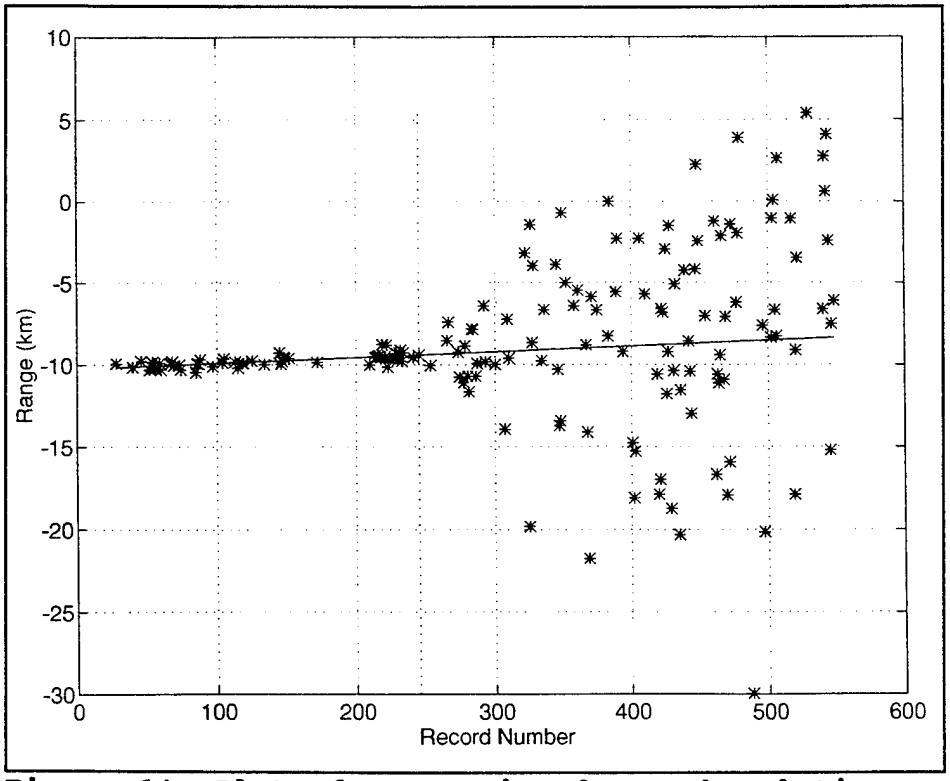

Figure 14. Plot of Range Bias for each solution (NPS #30) with line fit to determine systematic error.

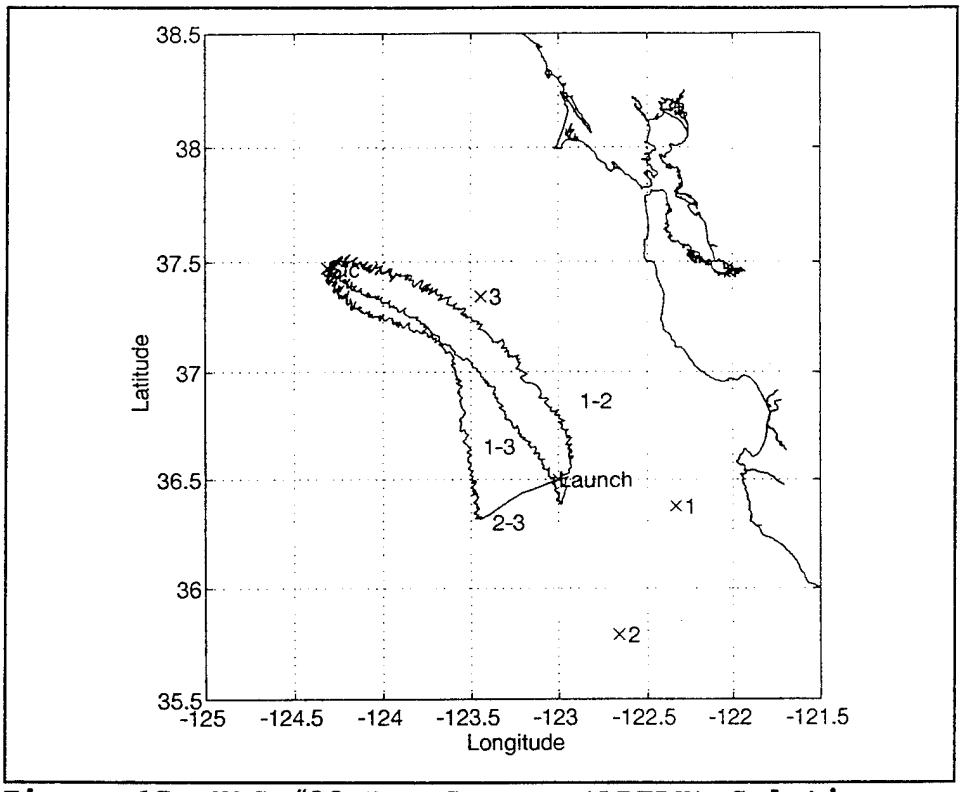

Figure 15. NPS #30 Two-Source (ARTRK) Solutions (source pairs indicated).

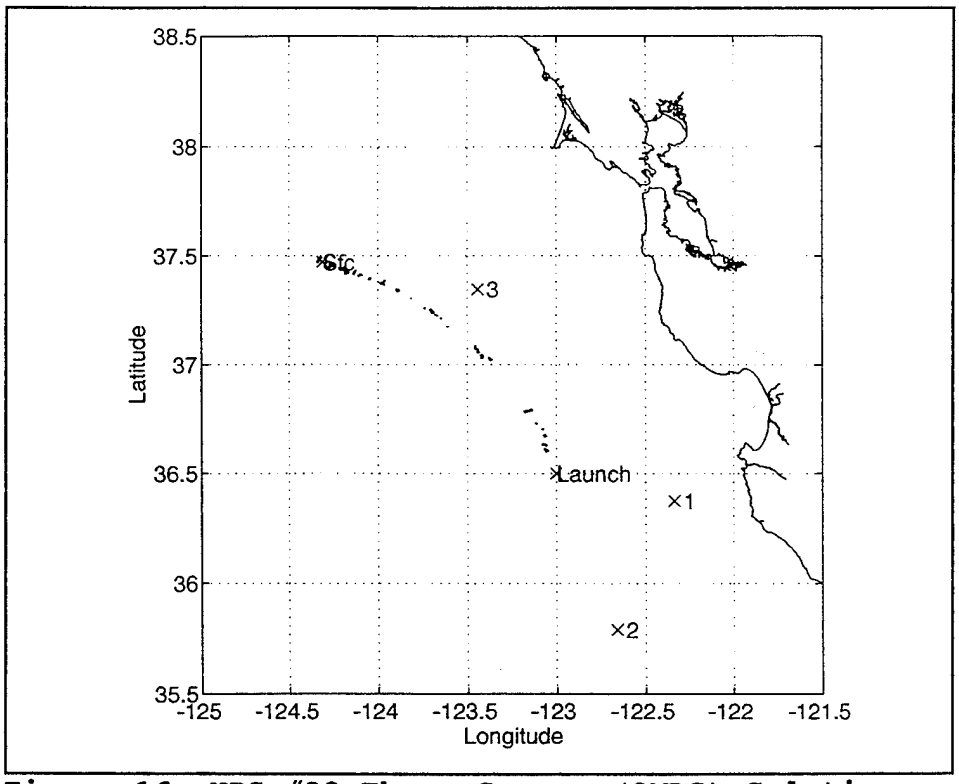

Figure 16. NPS #30 Three-Source (OMLS) Solution.

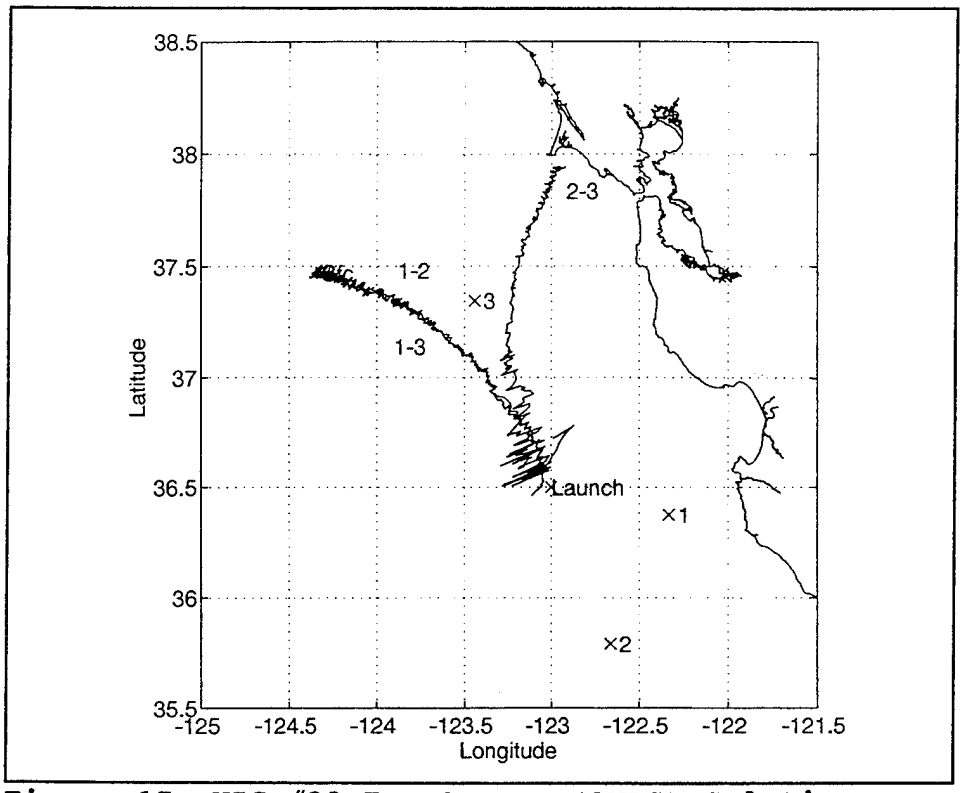

Figure 17. NPS #30 Two-Source (OMLS) Solutions (OMLS systematic error added)(source pairs indicated).

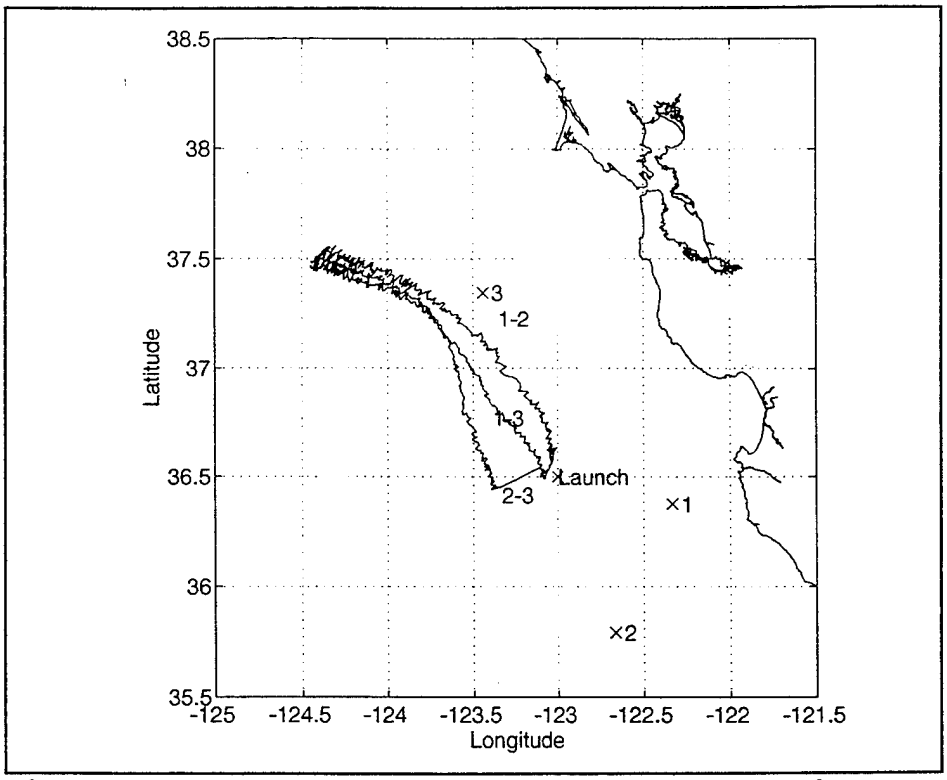

Figure 18. NPS #30 Two-Source (ARTRK) Solutions (OMLS systematic error added)(source pairs indicated).

IV. ANALYSIS

A. FLOAT TRAJECTORIES

Once launched and sunk to operational depth, the floats all drifted roughly northwest. The floats traveled at expected velocities, but at depths deeper than their anticipated target depths. Upon surfacing, they each drifted toward the south. Figures 15 through 28 show the subsurface tracks of each float determined from both the ARTRK and OMLS solutions and the ARTRK solution with the OMLS systematic error applied. Due to gaps in the data using the OMLS solution, lines only connect adjacent fixes throughout the trajectory. Figure 29 shows the surface trajectories after ARGOS acquisition. Each float was tracked on the surface for approximately two and a half months until transmitter shutdown.

Table 9 summarizes the percentage of available data out of 552 fixes that were available for each solution. Complete data sets were not always possible due to numerous reasons. The most significant reason is when the float drifted beyond the acoustic range during the 300-second window from a source. If the floats were left on deck (not actually launched) for any significant period (greater than one acoustic cycle) after float turn on, the float would still attempt to receive the acoustic signals from the sound sources, but of course would be unsuccessful, because the float was not yet in the water. When this occurs, the number of potential fixes decreases, as the float is programmed to record a specific number of fixes (in this case, 552). Another reason for incomplete data is that two of the floats were actually launched prior to the mooring of Source Three. Between this period, only two sound sources were available for acoustic fixing. Other gaps in the

records can be attributed to high ambient noise. One item to keep in mind when viewing Table 9 is for the two-source solutions, the gaps in the TOA records were interpolated, while in the three-source solutions they were not. Table 10 summarizes specific float parameters while descriptive information on each float follows.

FLOAT ID	TWO-SOURCE	THREE-SOURCE
NPS #21	47%	13%
NPS #22	65%	26%
NPS #24	100%	37%
NPS #30	100%	29%

Table 9. Percentage of data sets available for each solution type out of 552 fixes.

FLOAT ID	AVERAGE SUBSURFACE SPEED (CM S^{-1})	SUBSURFACE DISTANCE TRAVELLED (KM)	AVERAGE SURFACED SPEED (CM S^{-1})
NPS #21	13.0	247.5	18.5
NPS #22	9.3	183.5	20.7
NPS #24	7.6	148.9	12.6
NPS #30	8.1	160.2	17.3

Table 10. Float trajectory parameters.

1. NPS #21, Float Mickelinc

As can be seen in Figures 19 through 21, upon Float Mickelinc's launch, it drifted toward the northwest, proceeding along a track near Source Three. Once surfaced and acquired by System ARGOS, NPS #21 commenced a southerly drift (Figure 29). System ARGOS lost track of NPS #21 approximately 610 km southwest of San Diego, California. This float

solution did not track all the way to the surface point due to an incomplete data set (float window closed prior to receipt of acoustic signal from Sources One and Two).

For this particular float, it is difficult to determine which trajectory is the most probable. The OMLS solution (Figure 20) corresponds more closely with the Source One and Three ARTRK solution (Figure 19), but compares to the Source One and Two solution (Figure 21) with the OMLS systematic error applied. The reason for this discrepancy is that the float record is incomplete, and does not have subsurface fixes all the way to the surface point. A position for the last fix was estimated by trial and error using the three TOAs from the last fix to estimate a range from each source, then physically plotting circles of position around each source on a navigational chart. The position was assumed to be the center of the error triangle formed by the three circles. Because this position was not determined precisely (it was subject to human judgement), an additional position error was likely introduced, which carried into the final estimated solutions.

2. NPS #22, Float Arata

As can be seen in Figures 22 through 24, upon Float Arata's launch, it drifted toward the northwest, proceeding along a track to the south of Source Three. Once surfaced and acquired by System ARGOS, NPS #22 commenced a southerly drift (Figure 29). System ARGOS lost track of NPS #22 approximately 860 km southwest of San Diego, California. This float solution did not track all the way to the surface point again due to an incomplete data set (float window closed prior to receipt of acoustic signal from Sources One and Two).

Again in this float, an estimated position for the final fix was determined as described above for NPS #21. Figure 22 shows three distinct solutions from the ARTRK method. The OMLS solution (Figure 23) closely corresponds to the ARTRK

solution (Figure 21) from Sources One and Three. In the ARTRK solution with OMLS systematic error applied (Figure 24), the OMLS solution (Figure 23) compares with the solution from Sources One and Two. In Figure 24, a solution for Sources Two and Three was not obtained for reasons unknown, and the solution for Sources One and Three is the incomplete trajectory at the end of the trajectory for Sources One and Two. This discrepancy is again attributed to an imprecise position for the final fix of the float.

3. NPS #24, Float Feller

Float Feller (Figures 25 through 27) drifted toward the north approximately 30 km before it backed toward the northwest, proceeding along a track south of Source Three. Once surfaced and acquired by System ARGOS, NPS #24 commenced a southerly drift (Figure 29). System ARGOS lost track of NPS #24 approximately 550 km southwest of San Diego, California.

Unlike the previous two floats, this float has a complete data record from launch to surface. Here the OMLS solution (Figure 26) closely compares to the Source One and Two solutions in both the ARTRK solution (Figure 25) and the ARTRK solution with OMLS systematic error applied (Figure 27). In Figure 25, the Source Two and Three solution only consists of the end portion of the trajectory for reasons unknown. Thus, it is assumed that the solutions from Source One and Two are the most probable trajectory for this float.

4. NPS #30, Float Steger

Float Steger (Figures 15 through 18), drifted toward the north approximately 28 km before it also backed toward the northwest, proceeding along a track south of Source Three. Once surfaced and acquired by System ARGOS, NPS #30 commenced a southerly drift (Figure 29). System ARGOS lost track of NPS #30 approximately 610 km southwest of San Diego, California.

Like NPS #24, this float also has a complete record from launch to surface. Though the OMLS solution (Figure 16) does not closely compare to any of the three solutions from the ARTRK method (Figure 15), it does closely compare to the Source One and Two and Source One and Three solutions in the OMLS two-source solution with OMLS systematic error applied (Figure 17) and also the Source One and Two solution in the ARTRK solution with OMLS systematic error applied (Figure 18). It can be assumed that the Source One and Two solutions represent the most probable trajectory of this float.

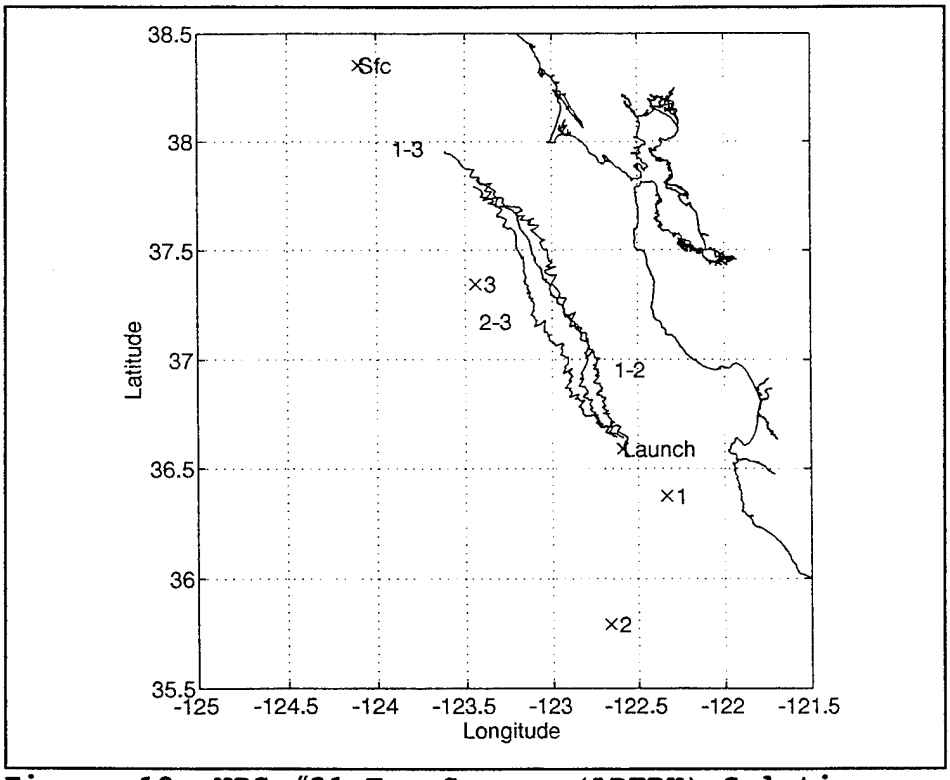

Figure 19. NPS #21 Two-Source (ARTRK) Solutions (source pairs indicated).

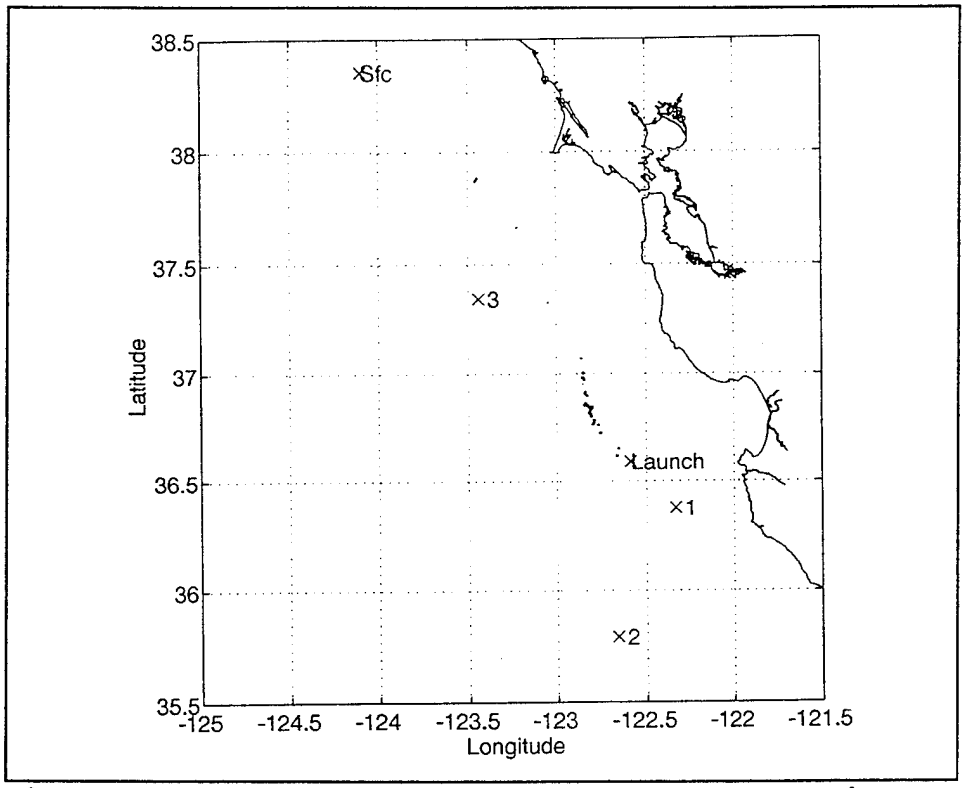

Figure 20. NPS #21 Three-Source (OMLS) Solution.

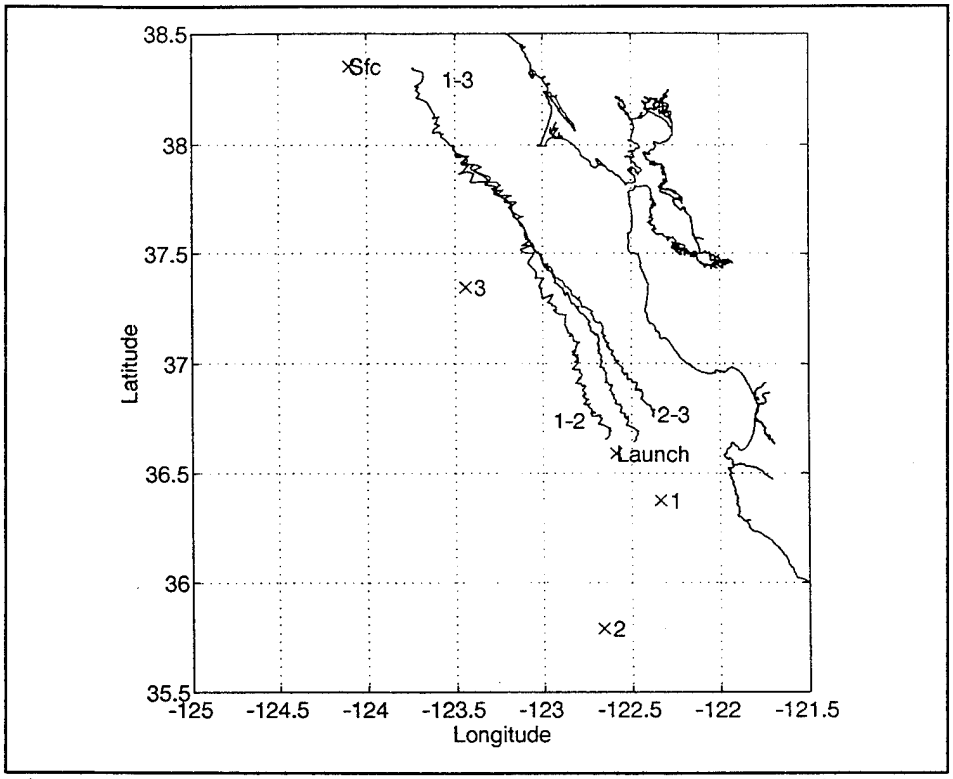

Figure 21. NPS #21 Two-Source (ARTRK) Solutions (OMLS systematic error added)(source pairs indicated).

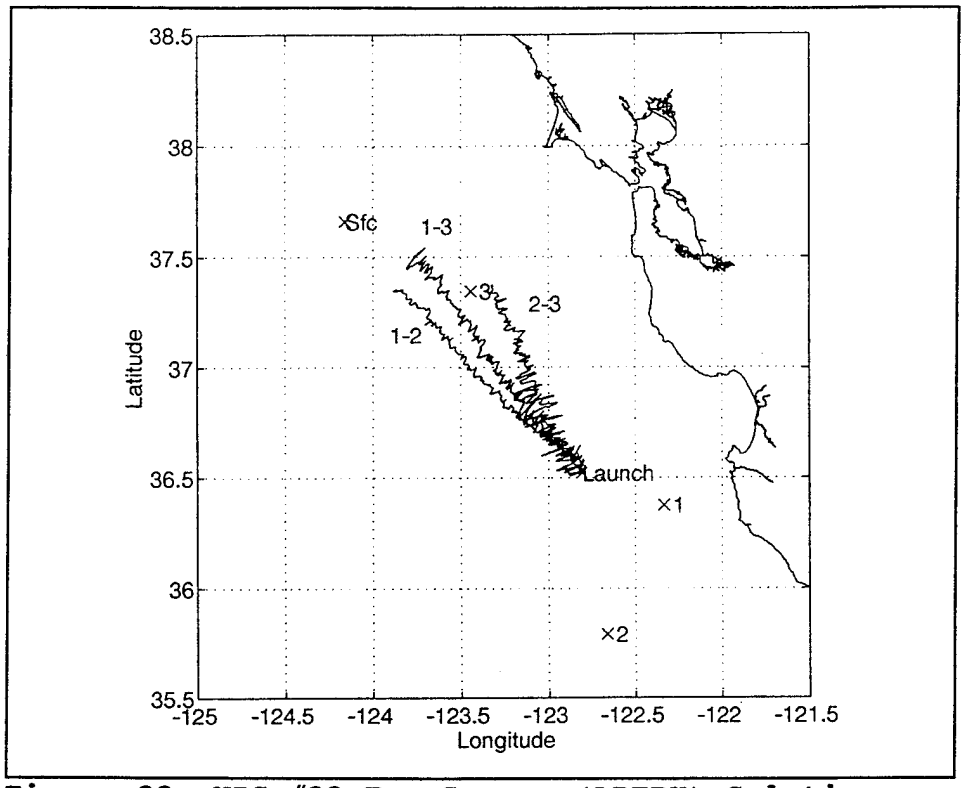

Figure 22. NPS #22 Two-Source (ARTRK) Solutions (source pairs indicated).

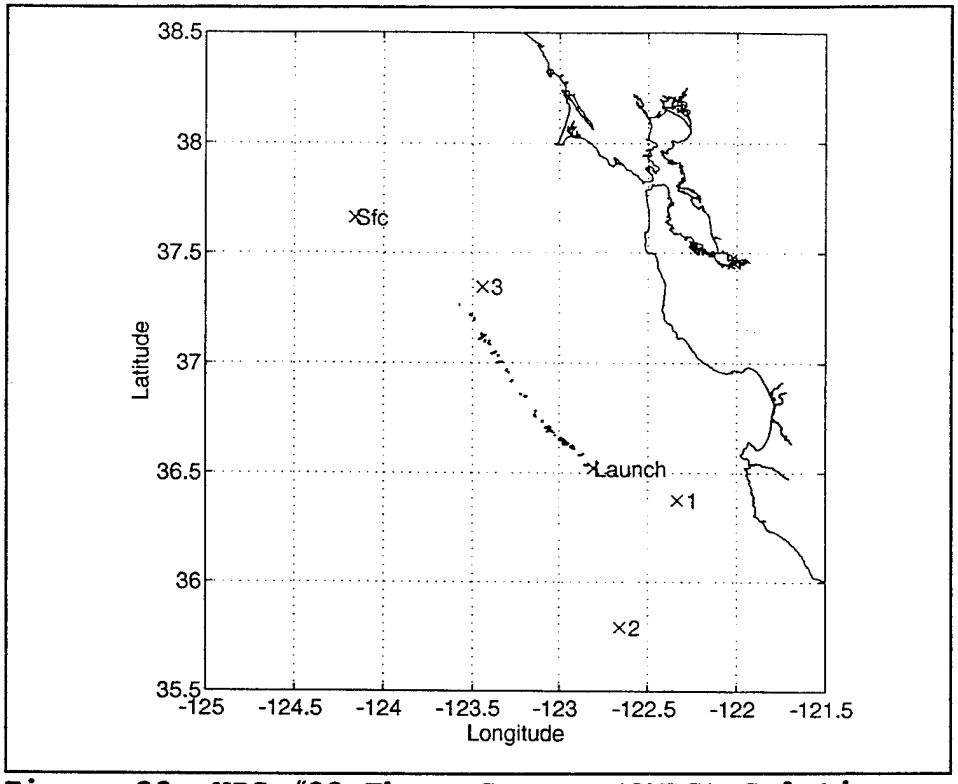

Figure 23. NPS #22 Three-Source (OMLS) Solution.

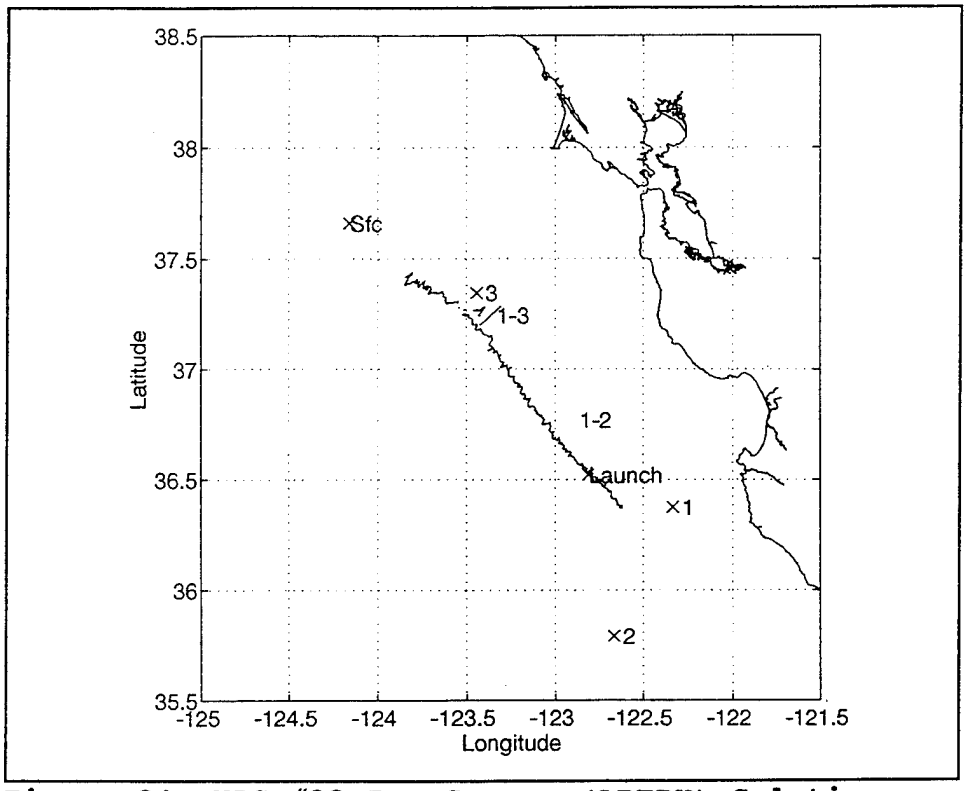

Figure 24. NPS #22 Two-Source (ARTRK) Solutions (OMLS systematic error added)(source pairs indicated).

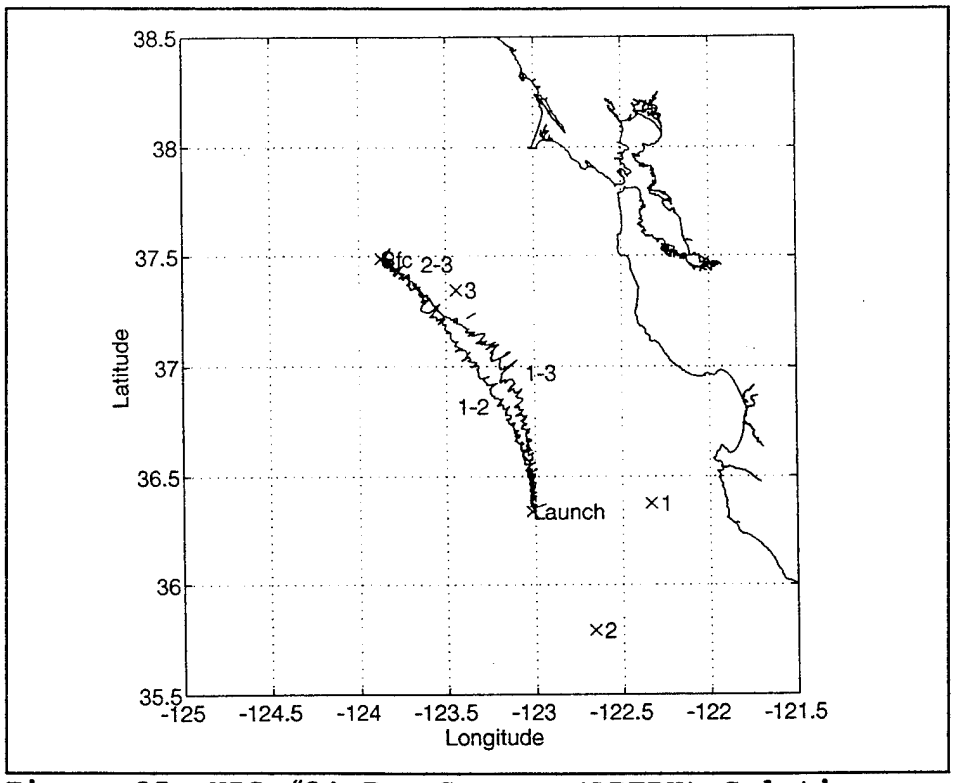

Figure 25. NPS #24 Two-Source (ARTRK) Solutions (source pairs indicated).

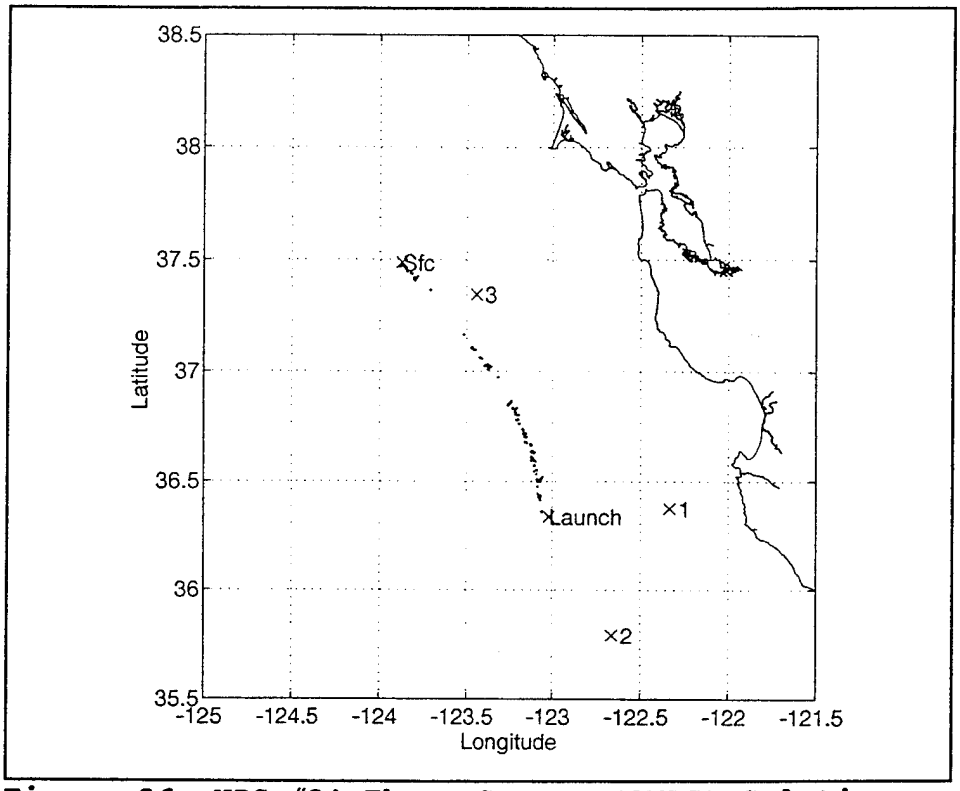

Figure 26. NPS #24 Three-Source (OMLS) Solution.

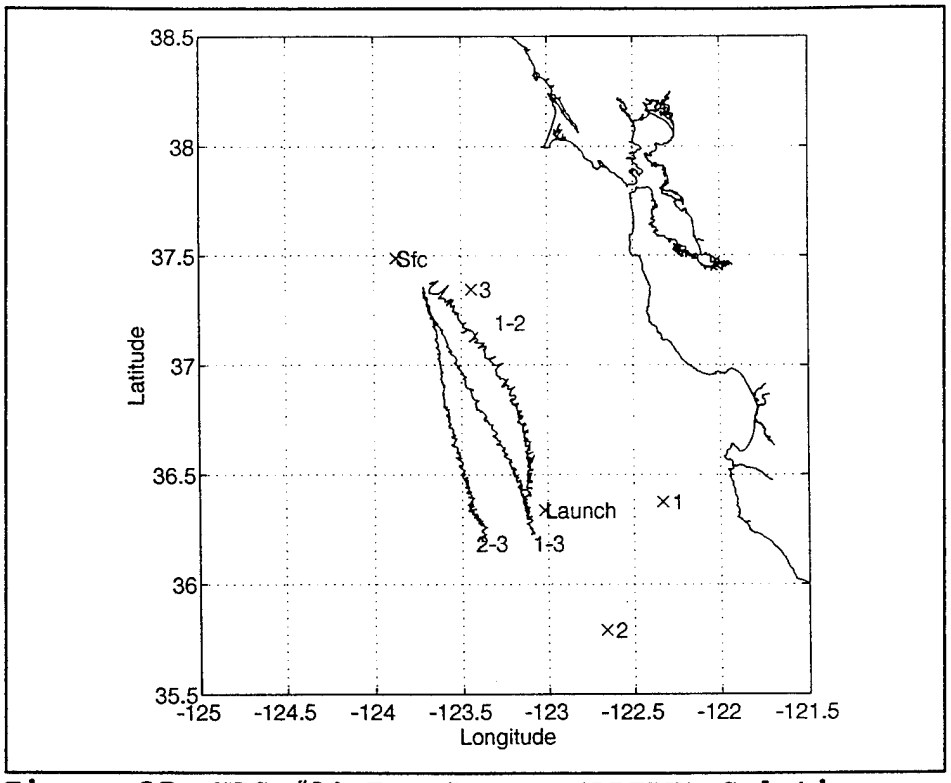

Figure 27. NPS #24 Two-Source (ARTRK) Solutions (OMLS systematic error added) (source pairs indicated).

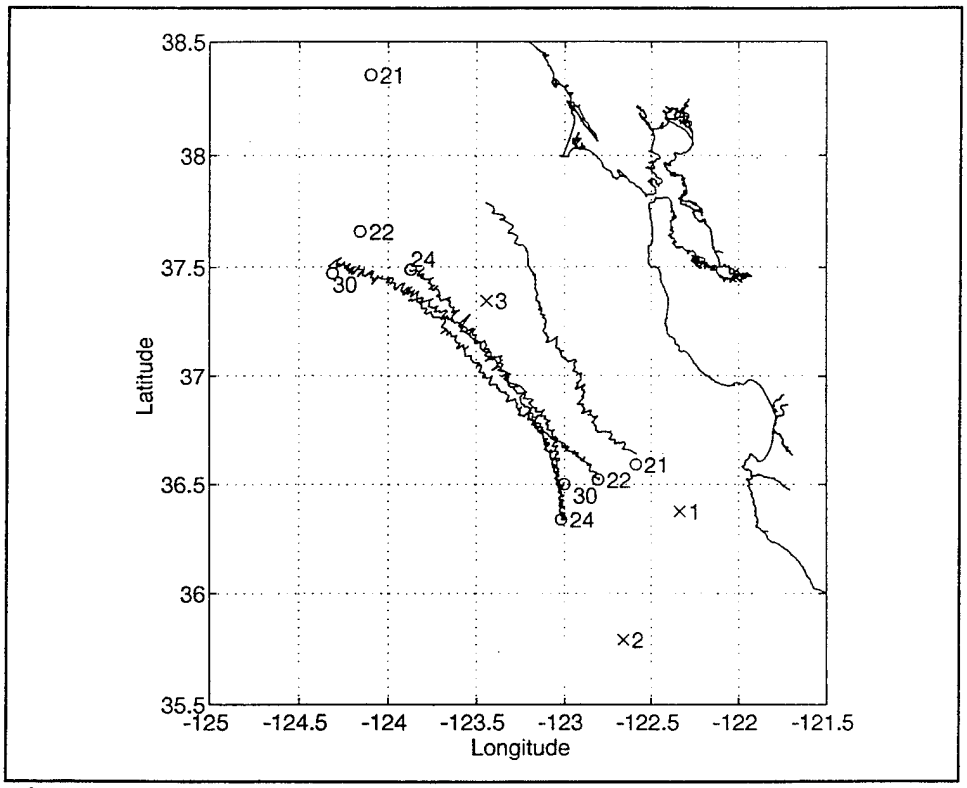

Figure 28. Subsurface trajectories, all floats.

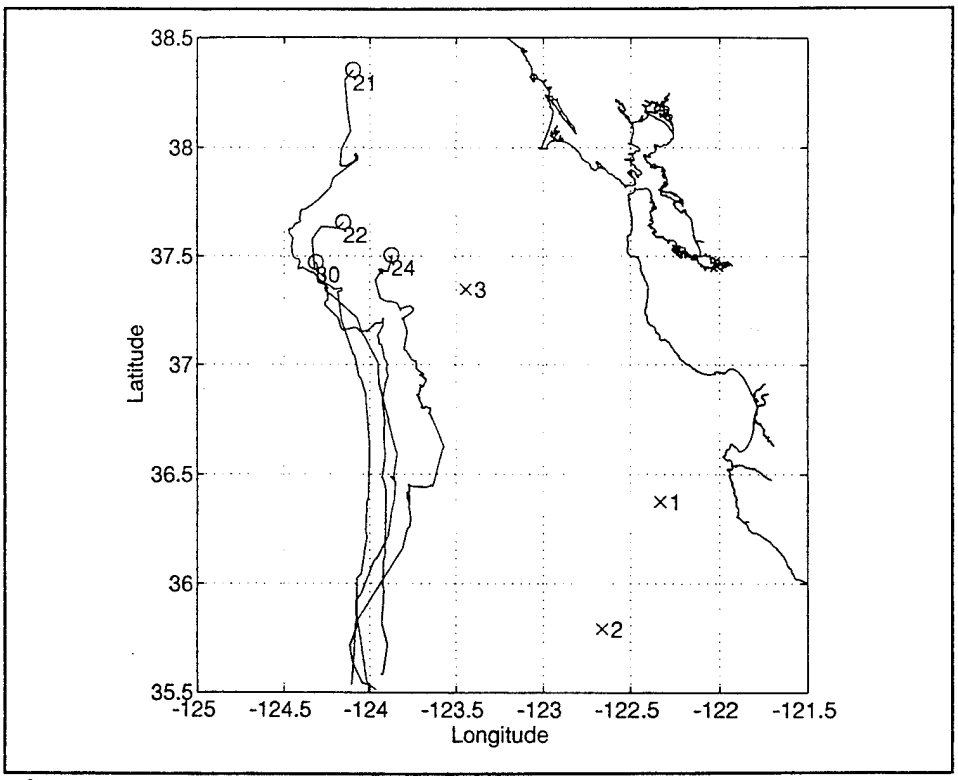

Figure 29. Surface trajectories, all floats.

B. TEMPERATURE, PRESSURE AND SALINITY

From each float, both temperature and pressure records were extracted showing the trend of each, respectively, throughout the three week mission. Recorded temperatures were consistent with recorded pressures when compared to CTD casts made near the source launch positions.

CTD records from the vicinity of source deployments, though not a valid record of stated parameters throughout the entire mission, can be used to give a general idea of what may be expected from each float at their specified depths. Table 11 lists the CTD Stations sampled prior to each of the three sound source launches.

SOURCE	CTD STATION	TIME/DATE	POSITION
1	1	0151Z 17 May 94	36° 23.57′ N 122° 20.77′ W
2	5	1146Z 17 May 94	35° 47.56′ N 122° 39.73′ W
3	10	1838Z 18 May 94	37° 20.02′ N 123° 27.24′ W

Table 11. CTD Station locations.

Figure 30 is a representative depiction of temperature, salinity and sigma-t (density anomaly) records versus depth for each CTD Station. This profile shows that temperature decreases with depth and salinity and density increase with depth at each station as expected. A closer look at each float follows with comparisons of float sensors to the CTD profile.

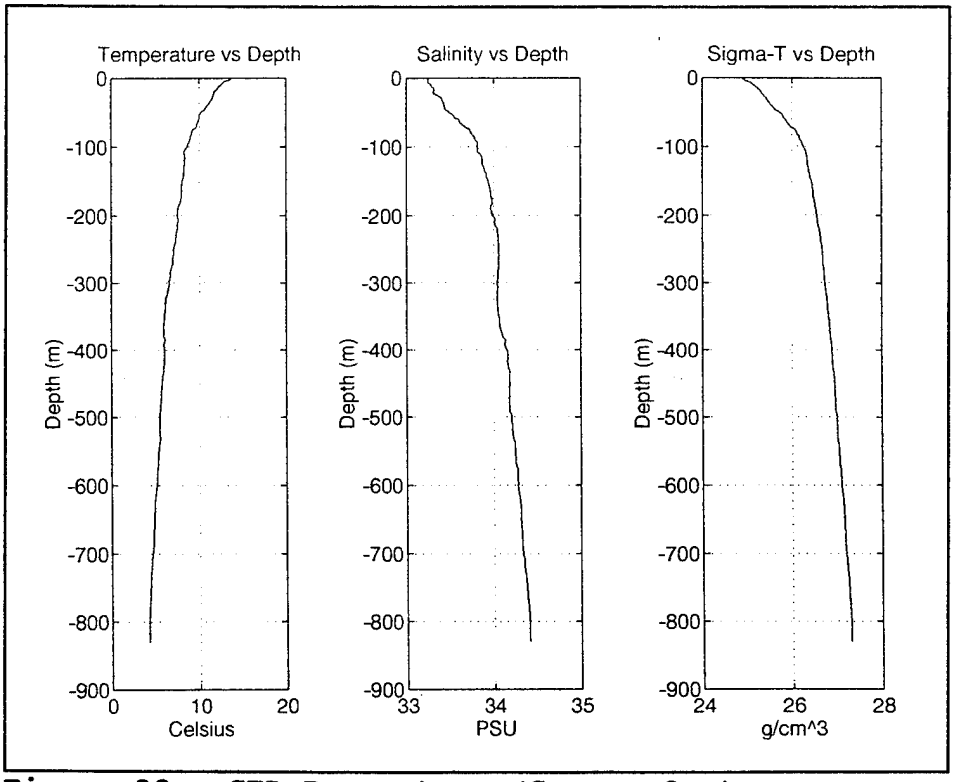

Figure 30. CTD Parameters (Source One). a) Temperature vs Depth, b) Salinity vs Depth, c) Sigma-T vs Depth.

Table 12 lists specific temperature values while Table 13 list specific pressure values recorded for each float. Figures 31 through 34 show the temperature and pressure records for each float. Further descriptions of temperature and pressure records of each float follow.

FLOAT ID	AVERAGE TEMPERATURE (°C)	MAXIMUM TEMPERATURE (°C)	MINIMUM TEMPERATURE (°C)
NPS #21	6.7	7.0	6.4
NPS #22	5.6	5.7	5.5
NPS #24	5.6	5.7	5.5
NPS #30	7.6	7.9	7.3

Table 12. Temperature Parameters for each float.

FLOAT ID	AVERAGE PRESSURE (dbars)	MAXIMUM PRESSURE (dbars)	MINIMUM PRESSURE (dbars)
NPS #21	363.0	390.0	336.0
NPS #22	577.0	592.0	565.0
NPS #24	547.0	560.0	531.0
NPS #30	289.0	303.0	273.0

Table 13. Pressure Parameters for each float.

1. NPS #21, Float Mickelinc

Throughout the mission of NPS #21 (Figure 31), the temperature recorded by NPS #21 tended to increase with time. On the average, an increase of approximately 0.3°C was realized. These values closely relate to the values expected when compared with the CTD data in Figure 30.

Because this float is drifting toward the north and suspected to be in the CUC, one might expect the temperature to decrease instead of increase with time due to cooler temperatures from the north. This can be explained when you analyze how the float drifts through the water. These floats are primarily isobaric floats, meaning they oscillate around a constant pressure level. Constant levels of density will cross this pressure surface, and as the float drifts farther north, density will decrease. If the float moves from a region of higher to lower density, the float will have to sink to remain on a constant pressure surface. The compression effects are greater than the density change due to the changing water mass, and the float depth change will generally be less than the change in depth of the isotherm. Hence, as a float moves to a region of less dense water, it will sink less than the depth change of the isotherm and the float will record a temperature increase.

In the pressure record (Figure 31), an increase of 10 dbars is realized throughout the mission. This increase can be explained as mentioned above concerning the float entering a water mass of lower density.

2. NPS #22, Float Arata

Throughout the mission of NPS #22 (Figure 32), the temperature recorded by NPS #22 tended to decrease with time. On the average, a decrease of approximately 0.05°C was realized. These values closely relate to the values expected when compared with Figure 30. This decrease in temperature is most likely due to contact with cooler water to the north.

In the pressure record (Figure 32), a decrease of 5 dbars is realized throughout the mission. This pressure decrease is expected as the temperature decreases. This suggests that the float moved into a region of denser water.

3. NPS #24, Float Feller

Throughout the mission of NPS #24 (Figure 33), the temperature recorded by NPS #24 tended to decrease with time. On the average, a decrease of approximately 0.07°C was realized. These values also closely relate to the values expected when compared with Figure 30. This decrease in temperature is most likely due to contact with cooler water to the north.

In the pressure record (Figure 33), a decrease of 5 dbars is realized throughout the mission. This pressure decrease is expected as the temperature decreases.

4. NPS #30, Float Steger

Throughout the mission of NPS #30 (Figure 34), the temperature recorded by NPS #30 tended to decrease with time. On the average, a decrease of approximately 0.3°C was realized. Again, these values closely relate to the values expected when compared with Figure 30. This decrease in temperature is most likely due to contact with cooler water to the north.

In the pressure record (Figure 34), a decrease of 10 dbars is realized throughout the mission. This pressure decrease is expected as the temperature decreases.

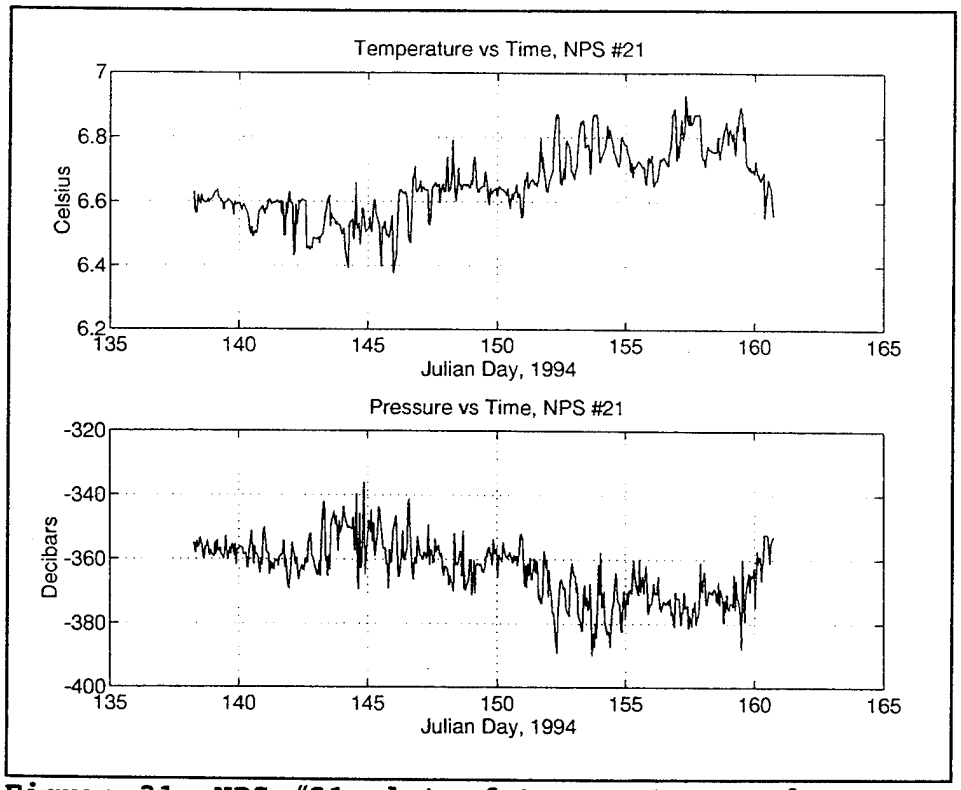

Figure 31. NPS #21 plot of temperature and pressure.

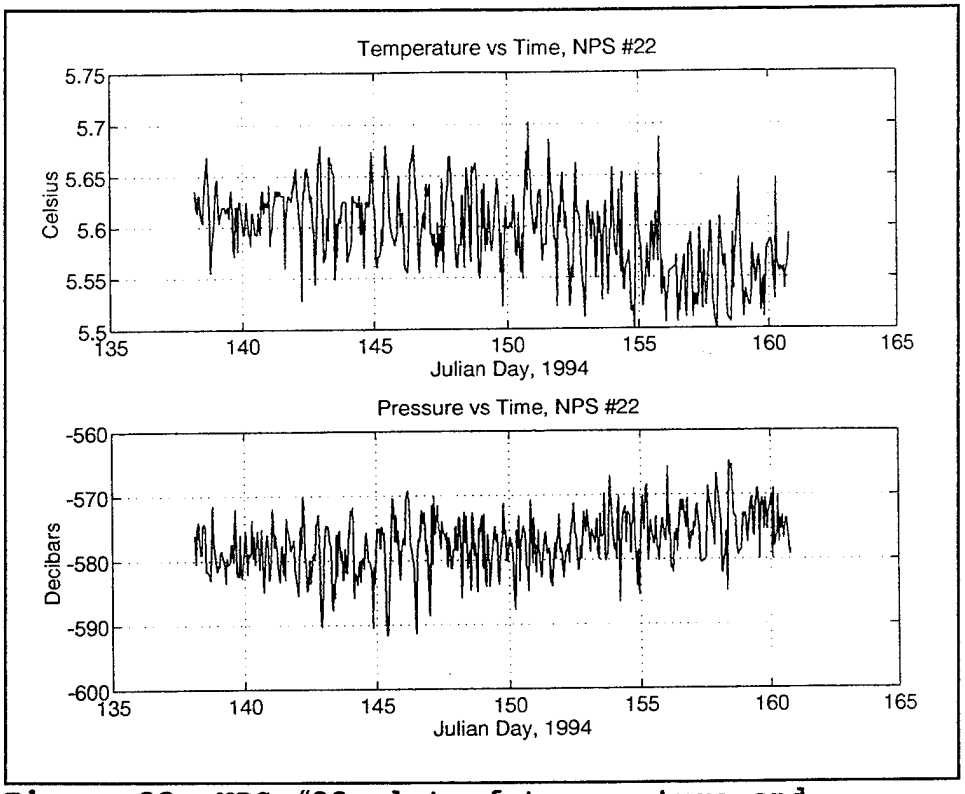

Figure 32. NPS #22 plot of temperature and pressure.

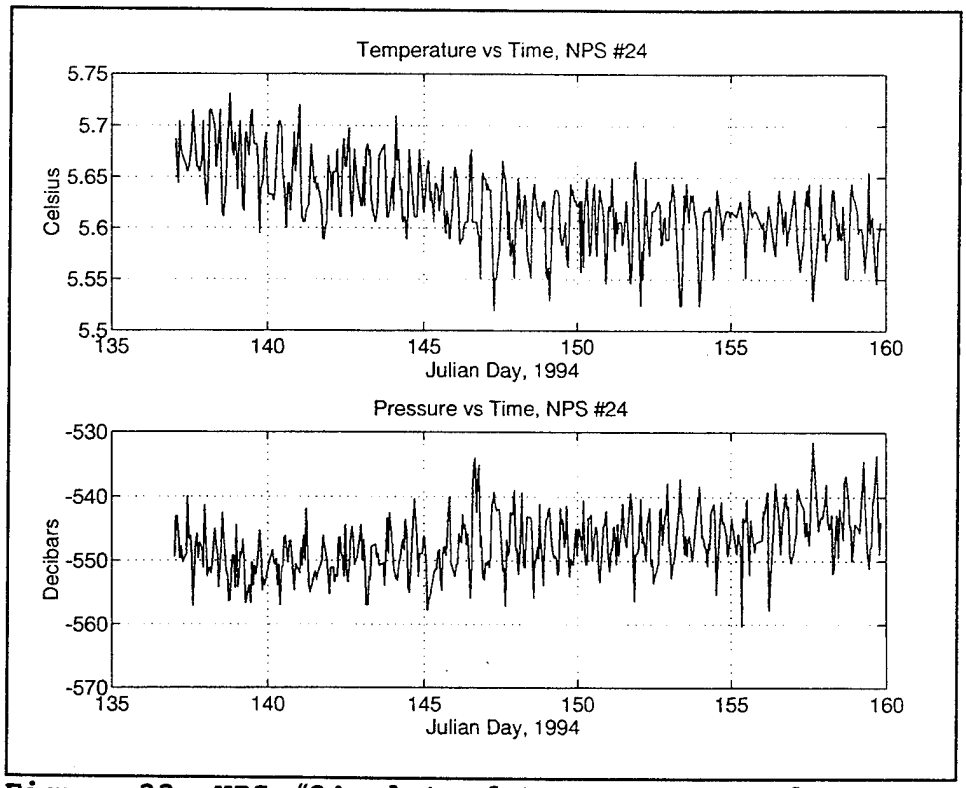

Figure 33. NPS #24 plot of temperature and pressure.

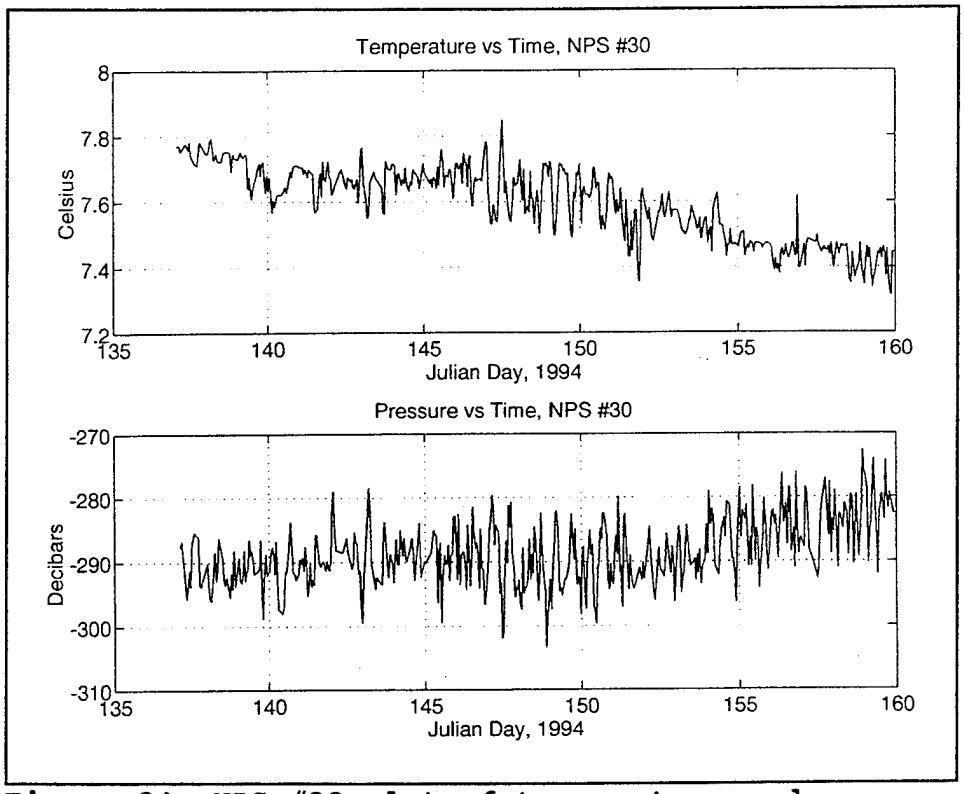

Figure 34. NPS #30 plot of temperature and pressure.

C. STABILITY

Figure 35 shows the calculated average Brunt-Väisälä Frequency or Buoyancy Frequency (N) for this region using the CTD data. As can be seen in this figure, N is positive, signifying this water column is stable, and it represents the upper limit of naturally occurring oscillations. At the depth of interest, N is approximately 2 cph. The Nyquist Frequency is thus 4 cph, or sampling needs to be done four times per hour. Since sampling was only done once per hour, it is not possible to resolve frequencies above .5 cph, and energy from higher frequencies could be aliased to lower frequencies.

The temperature and pressure variability (Figures 31 through 34) indicate oscillations of the float depth. The oscillations could be caused by internal waves, tides, weather patterns, or other forces affecting pressure.

Figure 36 shows a representative power spectrum on the temperature and pressure records for each float. The obvious spike at approximately 0.08 cph, which appears on the power spectra of all four floats, correlates to a period of about 12.5 hours. This is most likely the tidal period, but it could be another source of oscillation which has been aliased to this frequency.

Because the floats have a compressibility of approximately half that of water, the stability, E, for the floats will be about twice as much, hence the period, T, of the float, will be less, making the frequency of oscillation greater for the float (i.e., we expect to see more oscillations in the float). The magnitude of displacement will depend upon the magnitude of the displaced energy and inversely on E.

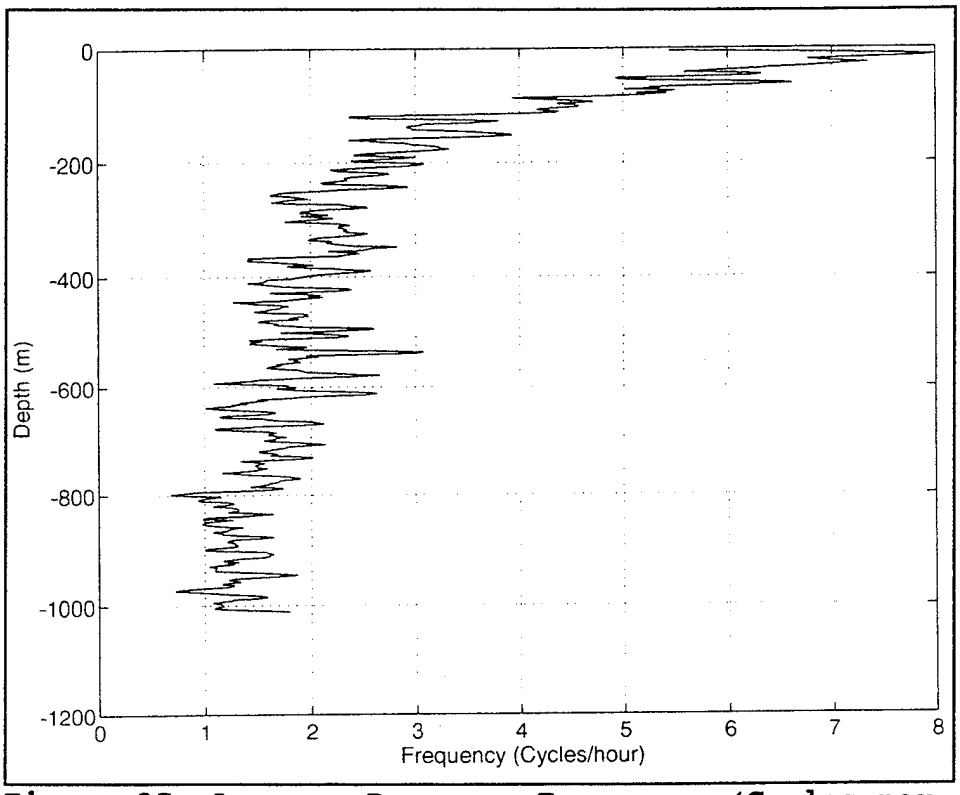

Figure 35. Average Buoyancy Frequency (Cycles per Hour).

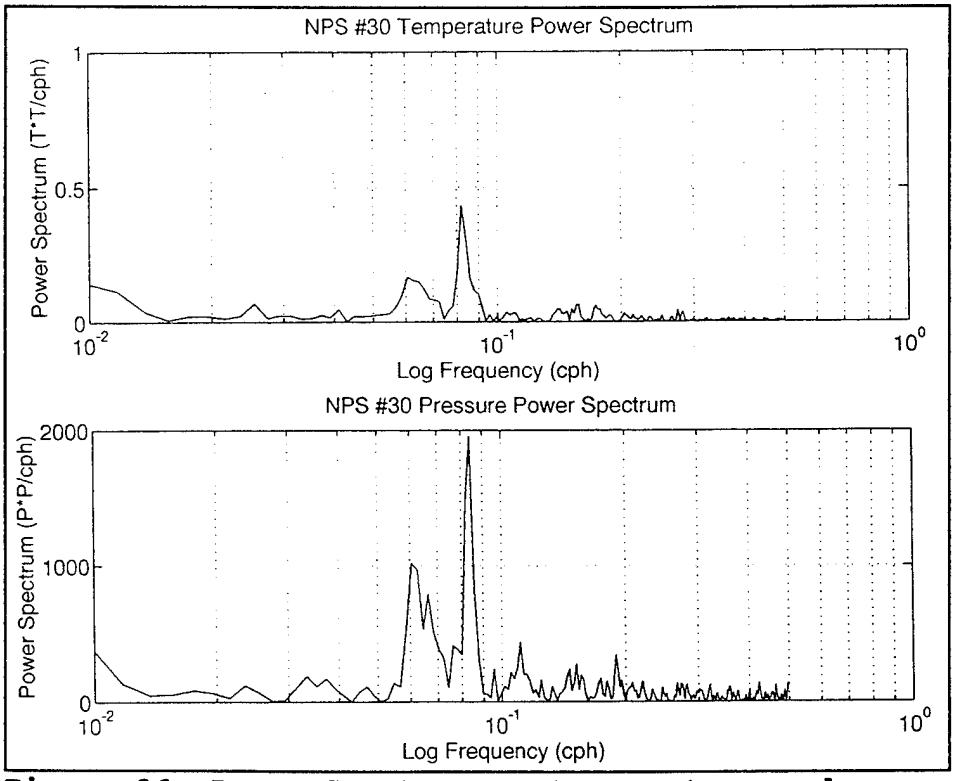

Figure 36. Power Spectrum on temperature and pressure (NPS #30).

D. SOLUTION COMPARISONS

In the ARTRK solution discussed by Paquette (1994), three solutions are available from three pairs of sources. Each TOA determines a circle of position. In general, two circles of position intersect at two points, reflected about the line between the two sources, of which only one is the correct position solution. Under good tracking conditions, we stay on the correct position along the track by solving the spherical navigational triangle by a method of successive approximations, starting with a previous good solution. This method fails when the float is too near the axis between sources or its extensions. This technique relies on a user inputed estimate for offsets and drifts (systematic error) as described previously.

In the OMLS solution discussed by Forsell (1991) and Clynch (1995), all three TOAs, from all the sources, are used. This method takes into account an estimated initial range and random error, and iterates until convergence at a solution. With this method, an actual systematic error is calculated, vice estimated. This error can then be used to input into a separate ARTRK solution, producing favorable results when a complete record is examined.

Ideally, the OMLS solution with OMLS systematic error applied should produce a more accurate solution; however with more gaps in the data, this solution has less data with which to work to obtain a float trajectory (Table 9).

V. DISCUSSION

To obtain an accurate navigational solution of a RAFOS float, it is imperative that all sources of potential error are identified and addressed. Without determining an estimate for the random and systematic errors, a plausible trajectory for the float will be difficult to achieve. Two methods have been discussed, each having different procedures to compensate for these errors, and their results have been seen.

The most difficult task in producing a navigational solution for a RAFOS float is the determination of a correct value for sound speed. This is especially true in the region of this study, as the existence of a sound channel cannot be confirmed.

In the traditional two-source ARTRK method, the random and systematic errors are estimated by matching the launch position with the first submerged fix (offset) and the surfacing position with the last submerged fix (drift). This combined correction adjusts for all of the errors; the significant ones being the variations of sound speed and the clock drift errors. This procedure relies on only two points, and often the last submerged fix is temporally offset from the first surfacing position. NPS #21 and NPS #22 are examples of this problem. In these cases, an offset can be estimated from the first submerged fix, but the drift cannot be estimated.

In the three-source OMLS method, the random errors are determined separately from the systematic errors by fitting a polynomial to the range data (TOAs). This value allows an estimation of the "goodness of fit" anticipated for each range when input into the solution. The iterative solution attempts to fit a solution within the error estimate allowed for each range. Since depth is input as a known variable in this method, the solution provides an estimate of the offset for every solution. Instead of having to rely on simply the start

and stop points of the submerged mission, an offset is determined for the entire data set. A linear regression of these offsets provides a more robust estimate of the offset and drift that does not depend on knowing the initial and final points. Since the OMLS solution will have fewer estimated fixes than ARTRK, the OMLS error estimate can be applied to the ARTRK method to obtain a more "mathematically correct" estimate of float positions, which includes the more robust error estimates for random and systematic errors. This method does not replace the ARTRK method, but rather improves it. By estimating this error based upon the complete data set instead of just the beginning and end points, another set of solutions with which to evaluate the most probable trajectory is available.

The float trajectories generally support results from previous studies, but also point out gaps in our understanding of the CCS. All four floats in this study traveled to the northwest during their submerged mission. NPS #21 was the most inshore, and traveled the fastest. It is speculated that this float was in the CUC or closer to the CUC core than the other three floats due to its higher speed. The motion of the other three floats is not as easily explained. The distance offshore would suggest that these floats were outside the CUC and in a region dominated by the CC. As such, a slow drift to the south would have been expected. Therefore, either the extent of the CUC is much broader than previously determined, or the flow of the water beneath the CC is not well understood. The drifts of these floats is not atypical (Newell Garfield, personal communication). Submerged floats not in the CUC tend to move northwest or westward with small velocities or get entrained in anticyclonic eddies and move generally westward or west-southwest. These floats suggest that at depths between 300 and 600 m, broad northerly flow is

not uncommon. This agrees with the mean currents between 250 and 500 m reported by Rischmiller (1993).

From satellite imagery during this period, meanders and upwelling were visible in the region; however because the CC is generally shallow (less than 300 m), the floats show no signs of being influenced by these features while submerged; however, once on the surface, the floats began to drift in a southerly direction, and were believed to be traveling in the CC in a meandering manner, as can be seen in Figure 29.

VI. CONCLUSIONS AND RECOMMENDATIONS

A. CONCLUSIONS

As can be seen in this study, the high sampling frequency of these RAFOS floats has proven beneficial in producing a detailed estimate of the trajectory over the short time span of the mission, when sources of error have been minimized. They have also allowed the study of numerous sources of error, especially the higher-frequency errors, which have the potential to degrade the final navigational solution.

For the evaluation of a final solution, a complimentary method has been proposed and demonstrated to determine and minimize systematic error calculated from the OMLS three-source technique on floats with complete data records from launch to surface. No longer is the traditional two-source ARTRK method of estimating a synthetic error the only option in estimating the float trajectory for the processor. With this estimate of systematic error, the navigational error is reduced, thereby allowing better correlation between the multiple solutions available. This error can then be applied to other solution methods to obtain additional float trajectory solutions to assist the processor in determining the most probable trajectory.

Both the ARTRK and OMLS solutions are acceptable processes to obtain a float trajectory; however, the ARTRK solution with OMLS systematic error applied is the most probable solution due to the larger number of range pairs. The OMLS solution with OMLS systematic error applied, though it has fewer data points, is a more accurate solution in certain portions of the trajectory where data are abundant due to being an overdetermined problem.

With a total potential RMS error on the order of 2 to 5 km, 1 cph sampling may be a bit of an overkill. This

frequency of sampling is too long to estimate vertical oscillations of the float and shorter than required for accurate velocity estimates, due to increased noise.

Because these floats were originally intended to support the Tomography Demonstration, this higher sampling rate may still be desirable for future tomography experiments despite the disadvantages stated here.

In this mission, these floats support and contribute to previous studies in determining the characteristics of the CC and the CUC. However, it appears that the CUC may be wider and deeper than previously suspected, as all four floats were influenced by a poleward flow wider and deeper than expected, based upon their separation distances and depths.

B. RECOMMENDATIONS

This study raises some important issues which require consideration.

- The floats used a five minute (300 seconds) window to receive the acoustic signals from the sound sources. With the floats in this study, as they drifted toward the north, they floated outside the acoustic range of Sources One and Two. If the windows were set to ten minutes (600 seconds), then the floats at their northern positions would have received the acoustic signals from the southerly sources, thereby preventing incomplete data records.

- Because the float acoustic cycle starts at nine minutes after the hour, the float should be turned on and launched at least ten minutes prior to time of the start of the acoustic cycle. Upon float turn on, it takes approximately ten minutes for the float electronics to warm up and run self diagnostics. If a float is launched that is not ready to receive its full cycle, data are being wasted.

- Future RAFOS data processors should be aware of the possibility of non-ideal sound propagation and be

prepared to deal with the resulting changes in effective sound speed. Since sound propagation cannot be known for certain between the source and the floats and sound speed likely is not constant, selecting a correct sound speed can be a difficult task. A sound speed of 1481 m s^{-1} can possibly be up to 15 m s^{-1} too high when taking into account the averaged sound speed in the entire water column.

- Sometimes operational requirements or weather conditions may not permit it, but all of the moored sound sources should be deployed prior to launching floats. Without the complete source geometry present, valuable data are not being considered.

- Prior to any float launching, a DOP Plot, as depicted in Figures 7 and 8, may prove useful in determining favorable launch positions to avoid poor navigational solutions when processing float data.

- In this study, all four floats were launched inside the triangle between the three sources. Future launches should avoid this strategy to avoid areas of higher DOP along the baselines of each source pair.

For further study, the following areas have significance for future research:

- A more detailed study into the actual systematic error determined from the MLS method could pinpoint specific causes of the error and increase the potential to reduce it.

- Comparing ARTRK solutions to OMLS three-source solutions after interpolating the data set, will remove the gaps in the data record and may prove beneficial.

- A study of the CUC to determine if it is wider than 20 km as previously suspected and how it relates to the anomalous poleward flow discovered by Rischmiller (1993) may conclude that the two poleward flows are related.

LIST OF REFERENCES

Bernstein, L.C., L. Breaker, and R. Whritner, 1977: California Current Eddy Formation: Ship, Air, and Satellite Results, *Science*, **195**, 353-359.

Bowditch, N., 1984: *American Practical Navigator*,Volume I, Publication No. 9, Defense Mapping Agency Hydrographic/ Topographic Center, Washington, DC, Article 4304, p 1016.

Brink, K.H. and T.J. Cowles, 1991: The Coastal Transition Zone Program, *J. Geophys. Res.*,**96**, 14,637-14,647.

Chelton, D.B., 1984: Seasonal Variability of Alongshore Geostrophic Velocity off Central California, *J. Geophys. Res.*, **89**, 3473-3486.

Clynch, J.R., 1995: *Parameter Estimation*, Mapping, Charting, and Geodesy (OC3903) Course Notes (Unpublished), Naval Postgraduate School, Monterey, California.

Eipp, T.B., 1995: *Differential GPS For Precision Approach: Commercial Technology and Navy/Marine Corps Requirements*, Master's Thesis, Naval Postgraduate School, Monterey, California, p 25.

Forsell, B., 1991: *Radionavigation Systems*, Prentice Hall, New York, New York, 392 pp.

Hickey, B.M., 1979: The California Current System - Hypotheses and Facts, *Prog. Oceanog.*, **8**, 191-279.

Huyer, A., P.M. Kosro, S.J. Lentz, and R.C. Beardsley, 1989: Poleward Flow in the California Current System, *Coastal and Estuarine Studies: Poleward Flows Along Eastern Ocean Boundaries*, Springer-Verlay, New York, New York, 142-156.

Johnson, R.H. and R.A. Norris, 1968: Geographic Variation of Sofar Speed and Axis Depth in the Pacific Ocean, *J. Geophys. Res.*, **73**, 4695-4700.

Knauss, J.A., 1978: *Introduction to Physical Oceanography*, Prentice-Hall, Inc., Englewood Cliffs, NJ, 338 pp.

Lynn, R.J. and J.J. Simpson, 1987: The California Current System: The Seasonal Variability of its Physical Characteristics, *J. Geophys. Res.*, **92**, 12947-12966.

Paquette, R.G., 1994: RAFOS Float Manual (Unpublished), Naval Postgraduate School, Monterey, California, 32 pp.

Pickard, G.L. and W.J. Emery, 1990: *Descriptive Physical Oceanography An Introduction*, Pergamon Press, New York, New York, 320 pp.

Podeszwa, E.M., 1976: *Sound Speed Profiles for the North Pacific Ocean*, Naval Underwater Systems Center, New London, Connecticut, 188 pp.

Pond, S. and G.L. Pickard, 1983: *Introductory Dynamical Oceanography*, Pergamon Press, New York, New York, 329 pp.

RAFOS Group, 1994: *RAFOS Float Technology Workshop Proceedings*, Woods Hole Oceanographic Institution, Woods Hole, Massachusetts, 115 pp.

Ramp, S.R., C.A. Collins, and R.G. Paquette, 1994: Currents Over the Upper Slope off Point Sur, California, 1989-1994, *CalCOFI Annual Conference 1994: Program and Absracts*, Lake Tahoe, California, 13.

Reece, R.H., 1989: An Analysis of Hydrographic Data Collected off Point Sur, California in November 1988, Master's Thesis, Naval Postgraduate School, Monterey, California, 75 pp.

Reid, J.L., 1962: Measurements of the California Countercurrent at a Depth of 250 m, *J. Mar. Res.*, **20**, 134-137.

Rischmiller, F.W., 1993: Variability of the California Current System off Point Sur, California from April 1988 to December 1990, Master's Thesis, Naval Postgraduate School, Monterey, California, 157 pp.

Rosenfeld, L.K., F.B. Schwing, N. Garfield, and D.E. Tracy, 1994: Bifurcated Flow From an Upwelling Center: A Cold Water Source for Monterey Bay, *Cont. Shelf Res.*, **14**, No. 9, 931-964.

Rossby, T. and D. Dorson, 1983: Instruments and Methods: The Deep Drifter-A Simple Tool to Determine Average Ocean Currents, *Deep-Sea Res.*, **30**, 1279-1288.

Rossby, T., D. Dorson, and J. Fontaine, 1986: The RAFOS System, *J. Atm. and Ocean. Tech.*, **3**, 672-678.

Sverdrup, H.U., R.H. Johnson, and M.W. Flemming, 1942: *The Oceans*, Prentice-Hall, Inc., Englewood, New Jersey, 1066 pp.

Tibby, R.B., 1941: The Water Masses off the West Coast of North America, *J. Mar. Res.*, **4**, 112-121.

Urick, R.J., 1983: *Principles of Underwater Sound*, McGraw-Hill Book Company, New York, New York, 423 pp.

Wickham, J.B., A.A. Bird, and C.N.K. Mooers, 1987: Mean and Variable Flow Over the Central California Continental Margin, *Continental Shelf Res.*, **7**, 827-849.

Wittman, P.A., E.A. Kelley, and C.N.K. Mooers, 1985: Hydrographic Data From the OPTOMA Program OPTOMA16 20 May - 23 June 1985, Technical Report, Naval Postgraduate School, Monterey, California, 125 pp.

Wooster, W.S. and J.H. Jones, 1970: California Undercurrent off Northern Baja California, 1978-1980, *J. Mar. Res.*, **28**, 253-260.

INITIAL DISTRIBUTION LIST

		No. Copies
1.	Defense Technical Information Center Cameron Station Alexandria, VA 22304-6145	2
2.	Library, Code 013 Naval Postgraduate School Monterey, CA 93943-5101	2
3.	Dr. Robert H. Bourke (Code OC/BO) Department of Oceanography Naval Postgraduate School Monterey, CA 93943-5000	1
4.	Dr. Newell Garfield (Code OC/GF) Department of Oceanography Naval Postgraduate School Monterey, CA 93943-5000	1
5.	Dr. Robert G. Paquette (Code OC/PA) Department of Oceanography Naval Postgraduate School Monterey, CA 93943-5000	1
6.	LT Kirk R. Benson, USN Department Head Class 141 Surface Warfare Officers School Command 446 Cushing Road Newport, RI 02841-1209	1
7.	Mr. Tarry Rago (Code OC/RG) Department of Oceanography Naval Postgraduate School Monterey, CA 93943-5000	1
8.	Director, Naval Oceanography Division Naval Observatory 34th and Massachusettes Avenue NW Washington, DC 20390	1
9.	Commander Naval Oceanography Command Stennis Space Ctr, MS 39529-5000	1
10.	Commanding Officer Naval Oceanographic Office Stennis Space Ctr Bay St. Louis, MS 39522-5001	1

11. Library 1
Scripps Institution of Oceanography
P.O. Box 2367
La Jolla, CA 92307

12. Dr. H. Thomas Rossby 1
Graduate School of Oceanography
University of Rhode Island
S. Ferry Road
Narragansett, RI 02882

13. Dr. Pierre Tilliet 1
Seascan, Inc.
Box 766, 13 County Road
North Falmouth, MA 02556